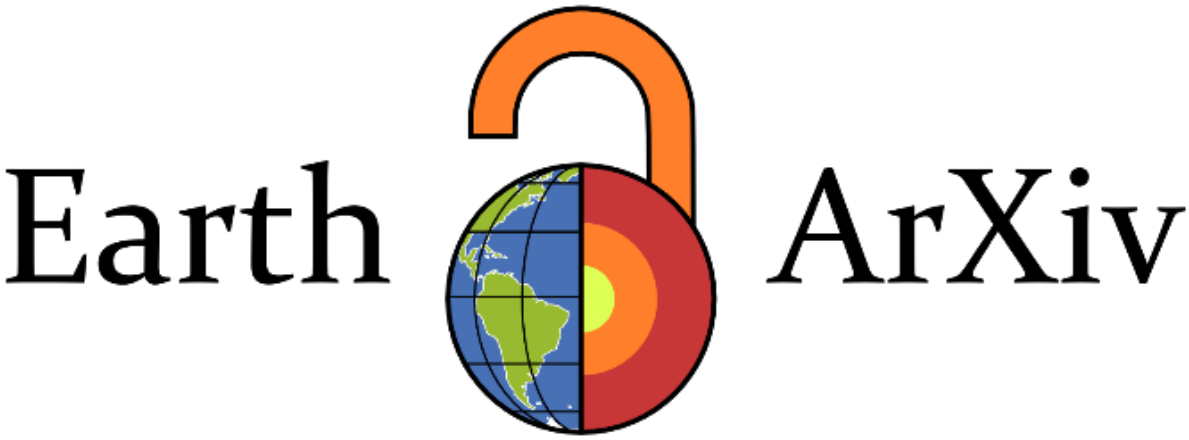

Evaluation and prediction of the Effects of Planetary Orbital Variations to Earth's Temperature Changes

Mengmeng Cao[1]†, Kebiao Mao[1]*†, Sayed M. Bateni[2], Jing M. Chen[3,4], Essam Heggy[5,6], Jong-Seong Kug[7], Xinyi Shen[8]

[1]State Key Laboratory of Efficient Utilization of Arid and Semi-arid Arable Land in Northern China, Institute of Agricultural Resources and Regional Planning, Chinese Academy of Agricultural Sciences, Beijing, 100081, China.

[2]Department of Civil and Environmental Engineering and Water Resources Research Center, University of Hawaii at Manoa, Honolulu, HI 96822, USA.

[3]School of Geographical Sciences, Fujian Normal University, Fuzhou, 350117, China.

[4]Department of Geography and Planning, University of Toronto, Ontario, Canada M5S 3G3.

[5]Viterbi School of Engineering, University of Southern California, Los Angeles, CA 90089, USA.

[6]Jet Propulsion Laboratory, California Institute of Technology, Pasadena, CA 91109, USA.

[7]Division of Environmental Science & Engineering, Pohang University of Science and Technology, Korea.

[8]School of freshwater sciences, University of Wisconsin Milwaukee, Milwaukee, WI, 53204, USA.

*Correspondence to: maokebiao@caas.cn

†These authors contributed equally to this work and should be considered co-first authors.

Declarations:

Conflict of Interest: The authors declared that they have no conflict of interest.

Funding: Key Project of Natural Science Foundation of Ningxia Department of Science and Technology (No. 2024AC02032), Fengyun Satellite Application Pilot Program "Development and Application of Fengyun all-weather Land Surface Temperature Spatiotemporal Fusion Dataset" (FY-APP-2022.0205).

Acknowledgments: The authors would like to thank the U.S. Department of Energy, Office of Science Biological and Environmental Research (BER), the National Oceanic and Atmospheric Administration Climate Program Office, the NOAA Physical Sciences Laboratory, and the European Centre for Medium-Range Weather Forecasts (ECMWF) for providing the climate reanalysis data, the Scripps Institution of Oceanography for providing the concentrations of CO2, the NASA Jet Propulsion Laboratory Developmental Ephemeris for providing the ephemerides for solar-system bodies, and the International Earth Rotation and Reference Systems Service Rapid Service/Prediction Centre for providing the daily length of day data.

Cover letter: Our paper "Evaluation and prediction of the Effects of Planetary Orbital Variations to Earth's Temperature Changes"is about the impact of planetary orbit changes on Earth's temperature changes. It was submitted to the journal Science two years ago and later to the journal Nature. We told editors that this work is very valuable and meaningful, and they tried to find relevant reviewers, but none of them were able to find suitable reviewers. They suggested that we submit the paper to a professional journal, but even after we switched to a professional journal, the editors still couldn't find suitable reviewers. The reason is that the research direction we are doing is a completely new direction that no one has done before. Although editors have invited more 40 reviewers, only one has accepted the review. The journal requires at least two comments, therefore it does not meet the requirements of the journal, and the editor suggests that we submit to other journals instead. Although a little previous analyses have been conducted, this work will comprehensively open up how we consider the impact of planetary orbit changes in climate change research, which will make this research a milestone. **Therefore, we have decided not to wait anymore because Earth ArXiv provides a great platform for showcasing research that is highly innovative and difficult to recognize at the moment, promoting progress and communication in new research directions. Many thanks for them and for you.**

Evaluation and prediction of the Effects of Planetary Orbital Variations to Earth's Temperature Changes

Mengmeng Cao[1]†, Kebiao Mao[1]*†, Sayed M. Bateni[2], Jing M. Chen[3,4], Essam Heggy[5,6], Jong-Seong Kug[7], Xinyi Shen[8]

[1]State Key Laboratory of Efficient Utilization of Arid and Semi-arid Arable Land in Northern China, Institute of Agricultural Resources and Regional Planning, Chinese Academy of Agricultural Sciences, Beijing, 100081, China.
[2]Department of Civil and Environmental Engineering and Water Resources Research Center, University of Hawaii at Manoa, Honolulu, HI 96822, USA.
[3]School of Geographical Sciences, Fujian Normal University, Fuzhou, 350117, China.
[4]Department of Geography and Planning, University of Toronto, Ontario, Canada M5S 3G3.
[5]Viterbi School of Engineering, University of Southern California, Los Angeles, CA 90089, USA.
[6]Jet Propulsion Laboratory, California Institute of Technology, Pasadena, CA 91109, USA.
[7]Division of Environmental Science & Engineering, Pohang University of Science and Technology, Korea.
[8]School of freshwater sciences, University of Wisconsin Milwaukee, Milwaukee, WI, 53204, USA.
*Correspondence to: maokebiao@caas.cn
†These authors contributed equally to this work and should be considered co-first authors.

Abstract: Existing climate studies mainly assessed the effect of greenhouse gases and aerosols, among other forcings on Earth's temperature. None of them has not evaluated the effect of the planetary orbital changes on Earth's temperature. Here, we deconvolved the effects of greenhouse gases and planetary orbital changes on Earth's temperature and to forecast the latter at different time scales. Our results suggest that Earth's revolution and rotation prompted ~75.4% and 15.9% of the observed Earth's intra-annual temperature changes, while Moon's revolution and other planet motions accounted for 8.3% and 0.3%, respectively. Planetary orbits contributed to ~11.5% of global warming since 1837 and will continue to warm the Earth by ~0.13 °C from 2020 to 2027. However, planetary orbits may trigger ~0.25 °C of Earth's cooling from 2027 to 2050, which is still far below the impact of CO_2 and will not be enough to reverse the warming trend.

Main Text: Changes in Earth's temperature (i.e., the average global temperature) govern the evolution of its climatic, biological and hydrologic conditions, which in turn define the planet habitability for both humans and organisms [1-4]. Earth's temperature has risen by approximately 1.37 °C and 0.86 °C since 1836 and 1979, respectively, mostly attributed to the increase in greenhouse gases [5-8]. Six separate assessment reports from the United Nations (UN) Intergovernmental Panel on Climate Change (IPCC) during the last decades concluded that global warming is mainly driven by greenhouse gas emissions due to human activities [9-14]. Only the fifth and sixth IPCC reports quantified the human-induced contribution to the observed temperature change using long-term observational datasets and improved climate models.

The concentration of greenhouse gases in the atmosphere has risen monotonically since 1836, while Earth's temperature records show significant oscillations over the same period. Additionally, the rise in Earth's temperature appears to be part of a long-term warming that began before the industrial era in the 17th century [15,16]. Moreover, paleoclimate data from various sources (e.g., ice cores, deep-sea sediments, tree rings, pollen, corals and glaciers) demonstrate preindustrial temperature oscillations [17-22]. Taken together, these observations imply that the drivers of global warming are complex and that other factors can modulate the greenhouse gas effect.

Planetary orbital changes have been important drivers of temperature variation throughout Earth's evolution as they impact heat transfer from the sun to the upper atmosphere [23-26]. While these orbital changes are minor and account for a few centimeters per year [23,24,26-28], their integrated effect over the last 185 years on the changes in global temperature can be examined if we successfully deconvolve the augmentation caused by greenhouse gases. Unlike the steady increase in greenhouse gas concentrations in the atmosphere over the past 185 years that has continuously increased Earth's temperature, the effect of planetary orbits on Earth's temperature is complex. The external gravitational forces acting on the Earth during its revolution vary due to planetary geometry, ultimately perturbing the orbital geometry of Earth [26-28]. Some basic parameters of Earth's orbit, such as eccentricity, axial tilt, and the precession of equinoxes, vary cyclically, resulting in complex interactions among various components of the Earth's system and therefore periodically changes Earth's temperature [27,29-31]. For example, Earth's temperature has different cycles of approximately 100000, 40000, 20000, 2100−2500, 1200−1800, 200, and 50−70 years, which are in phase with the cycles of gravitational perturbations induced by planets of the solar system, primarily Jupiter, Moon, Uranus, Neptune and Saturn [28,31-36]. Therefore, their positive contribution can exacerbate anthropogenic warming of Earth. In contrast, a negative contribution of planetary orbits to Earth's temperature can attenuate human-induced warming for a short time-scale, causing oscillations in Earth's temperature. While existing studies have highlighted that the Earth's climate system is modulated by a number of astrodynamical phenomena [37-39], they did not quantify the effect of the changes in planetary orbits on the Earth's temperature changes.

To address this deficiency in comprehensive assessment of Earth's temperature variation, we developed a conceptual framework to investigate the effect of different planetary orbits on Earth's temperature change from 1836 to 2020 for different time scales. For this purpose, we first eliminated the influence of greenhouse gases on the Earth's temperature and built several mathematical models that quantify the contribution of different planetary orbital variations to Earth's intra-annual temperature changes. A conceptual diagram showing the effect of different orbits on the Earth's intra-annual temperature is shown in Fig. 1. The Earth's rotation and the Moon's revolution around the Earth affect the temperature on the daily and lunar sidereal periods, respectively. Their influence on the Earth's intra-annual temperature is represented by the sinusoidal-like function f_1 and the irregularly changing function f_2, respectively (see Fig. 1). Considering only the Earth-Sun system, the influence of the Earth's revolution around the Sun on the Earth's intra-annual temperature can be represented by the function f_3 in Fig. 1. The curves f_1, f_2, and f_3 are superimposed to find the simultaneous effects of Earth's rotation, Moon's revolution around Earth, and Earth's revolution around the Sun on Earth's temperature during each year.

The motions of the other seven major planets in the solar system (namely, Mercury, Mars, Jupitar, Saturn, Neptune, Venus and Uranus) have a subtle impact on the Earth's temperature on intra-annual and interannual time scales, as shown by the functions Z_1-Z_7 in Fig. 1. Mathematically speaking, their influence on the Earth's temperature can be taken into account by superimposing the functions Z_1-Z_7 on the curves $f_1 - f_3$. Furthermore, we quantified the respective impacts of planetary orbital changes and CO_2 concentrations (the dominant greenhouse gas) on Earth's temperature changes on an interannual time scale by developing a robust mathematical model. In addition, a hybrid model was developed based on the long short-term memory (LSTM) and spectral domain approaches to forecast the effect of planetary orbits on Earth's temperature. This study advances our understanding of the influence of planetary orbits and CO_2 concentrations on Earth's temperature over a wide range of time scales from hours to years. This understanding is of

great importance for analyzing future climate change and assessing climate change mitigation policies and sustainable development practices.

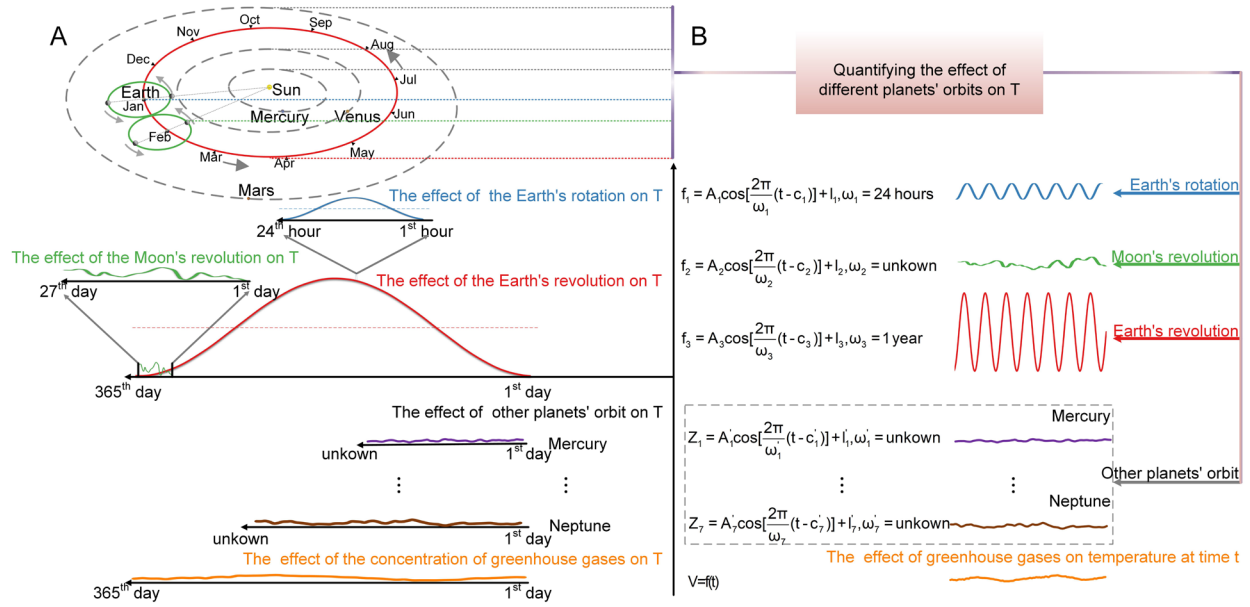

Fig. 1. A simplified diagram showing the effects of different planetary orbits on the Earth's temperature (T), which consists of two parts: (**A**) Physical based on our knowledge of the separation between the sun and the earth (**B**) the proposed mathematical method to quantify the effect of different planetary orbits on (A) and hence on the Earth's temperature.

Results

The physical response of Earth's temperature to different orbits

Our analyses reveal that the Earth's temperature variation over different time scales is related to the Earth's motion state (its revolution and rotation) and, to a lesser extent, the other planets' orbital motions. Since the variation of the solar-induced temperature is negligible during each Earth's rotation [40], the quasi-sinusoidal diurnal variation in Earth's temperature (Supplementary Fig. S1) is mainly due to the uneven distribution of land and sea on the Earth's surface causing a difference in surface albedo. The change in the Earth's temperature in two successive hours is due to the variations in the land temperature (see Section 1.1 in the Supplementary Materials for further details). By analyzing the temporal variations in daily lunar declination (δ), Earth-Moon distance, Earth's temperature and Earth's rotation data from 1979 to 2020 (Supplementary Fig. S4), it is found that lunar declination and Moon-Earth distance can indirectly influence Earth's temperature by affecting the speed of Earth's rotation (see Section 1.2 in the Supplementary Materials for more information). Additionally, the slow periodic changes in the solar declination and, to a much lesser extent, the Sun-Earth distance mainly cause seasonal and latitudinal variations in insolation, leading to changes in the Earth's temperature during a year (see Section 1.3 in the Supplementary Materials). In addition, the up and down swing of the Sun's position relative to the equatorial plane (caused by the revolution of the Earth) triggers the seasonal variation of the Earth's rotation in each year (weak deceleration (72 days), strong acceleration (110 days), strong deceleration (109 days), and weak acceleration (66 days)), which also contributes to oscillations of the temperature difference between two successive days (Supplementary Fig. S4C). The Fourier transform analysis (Supplementary Table S1) of the annual mean Earth's temperature from 1836 to 2020 also shows

that planetary motion may have indirectly impacted the interannual Earth's temperature by affecting Earth's orbit and velocity (Supplementary Section 1.4).

Contribution of planetary orbits to changes in Earth's temperature during the year

The developed mathematical model (see Section 1 in Methods) is merged with historical temperature data to determine the contribution of planetary orbits to Earth's intra-annual temperature changes. Fig. 2A shows that the orbital forcings (i.e., Earth's revolution around the Sun, Earth's rotation, Moon's revolution around the Earth and other planet motions) cause ~ 99.79% of the temperature change during the year (1979−2020), while the contribution attributable to other factors (e.g., changes in greenhouse gas concentrations, other human drivers due to aerosols, ozone and land-use change) is only approximately 0.21%. Earth's revolution, Earth's rotation, the Moon's revolution, and other planet motions contribute ~ 75.36%, 15.91%, 8.26% and 0.26% to the intra-annual Earth's temperature change during 1979−2020, respectively (Fig. 2A). Fig. 2B shows the annual Earth's temperature variations due to different orbital forcings and other factors from 1979 to 2020. In this figure, temperature changes are color coded based on their kernel density. The observed maximum annual temperature change (i.e., the difference in the maximum and minimum hourly temperatures in that year) from 1979 to 2020 is approximately 4.73–5.46 °C, with a mean of 5.06 °C. The ranges of temperature variations induced by the Earth's revolution, Earth's rotation, the Moon's revolution, and the motion of the planets are 3.56–4.15, 0.78–0.82, 0.36–0.47, and -0.25–0.23 °C, respectively, with means of 3.81, 0.81, 0.41 and 0.01 °C (Fig. 2B). The total temperature changes due to other factors (e.g., changes in greenhouse gas concentrations, other human-related drivers including aerosols, ozone and land-use change) are ~ 0.01 °C (Fig. 2B).

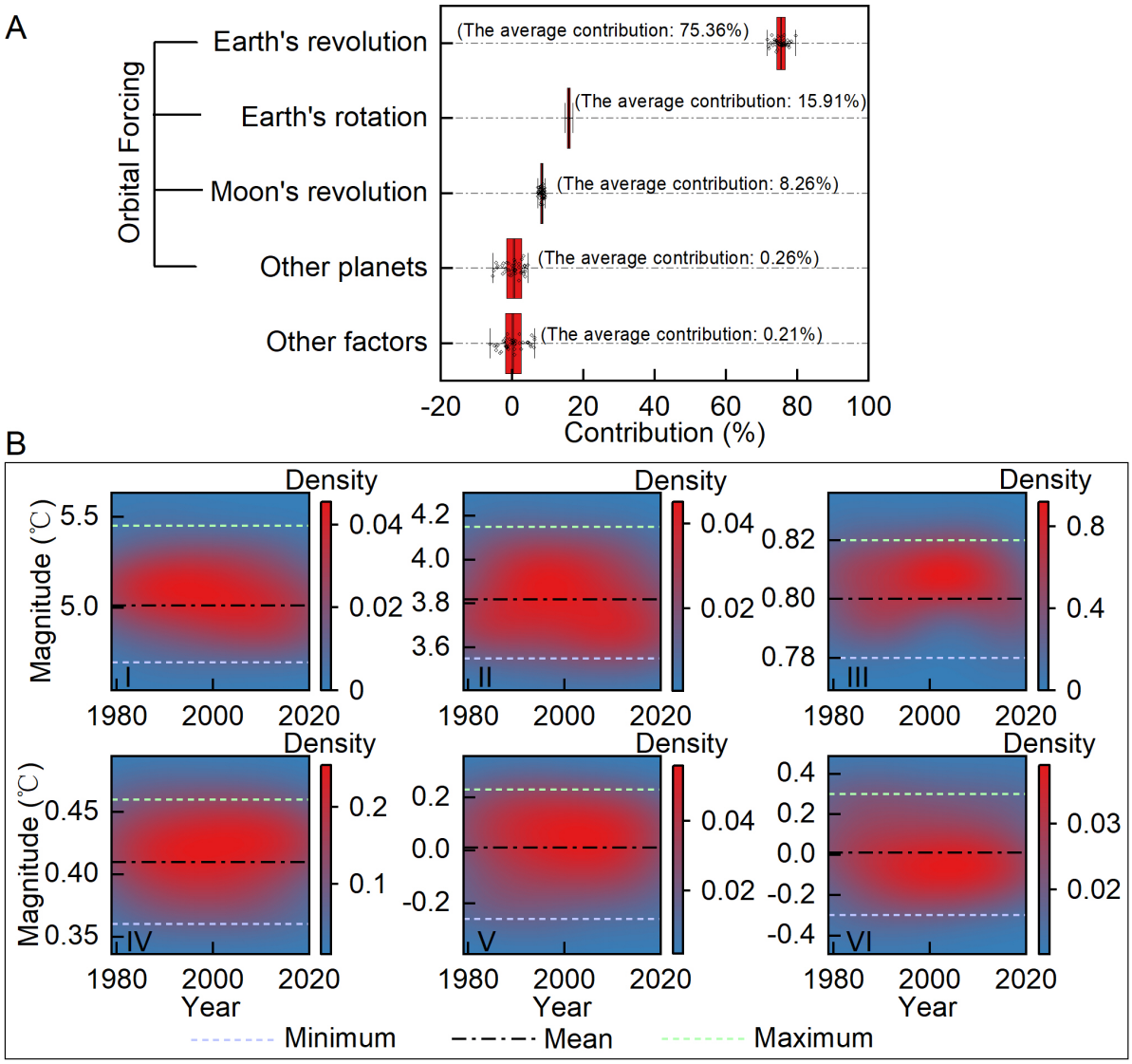

Fig. 2. (**A**) Boxplot of the contributions of various planetary orbits and other factors (e.g., changes in greenhouse gas concentrations, other human-related drivers including aerosols, ozone and land-use change) to the Earth's intra-annual temperature changes during 1979−2020 (boxplot: middle line, median; box, interquartile range (IQR); whiskers, 1.5xIQR). (**B**) The magnitude of the annual Earth's temperature variations in response to (II) Earth's revolution, (III) Earth's rotation, (IV) Moon's revolution, (V) other planets, and (VI) other factors from 1979 to 2020, and (I) is the observed maximum Earth's annual temperature change over the period 1979−2020. The Earth's temperature changes in each plot are color coded based on their kernel density. The dashed blue, black, and green colors represent the minimum, mean, and maximum of Earth's temperature changes.

Based on our developed mathematical model, every 26.8° of the Earth's orbit around the Sun (i.e., approximately one sidereal month), 15° of the Earth's rotation (i.e., approximately one hour), and 13.2° of the lunar revolution around the Earth (i.e., approximately one day) cause the Earth's temperature to vary over the ranges of -1.295–1.163, -0.404–0.3, and -0.192–0.221℃ with means of 0.634, 0.069, and 0.041℃, respectively.

Contribution of planetary orbits to changes in Earth's temperature on an interannual scale

We quantified the contribution of planetary orbits and CO_2 concentrations to Earth's temperature changes from 1837 to 2020 using the year 1836 as the benchmark (Fig. 3A). The contribution of planetary orbits to the interannual variations in Earth's temperature was dominant (more than 50%) before 1920, with the highest value of 97.6% in 1837. On the other hand, interannual changes in the Earth's temperature were mainly controlled by the increase in CO_2 concentration after 1920, especially in the last two decades. Notably, the contribution of CO_2 to Earth's warming from 2000–2020 was approximately 86% (see Section 2 in Methods).

Figure 3B compares the influence of planetary orbits on the Earth's temperature with that of the CO_2 concentration from 1837 to 2020. We developed a hybrid forecast model based on LSTM and a spectral domain approach to forecast the effect of planetary orbits on Earth's temperature over 2021-2050 using historical values over 1837-2020 (Fig. 3B; see Section 3 in Methods). Five conclusions can be drawn from this figure: (1) the influence of planetary orbits on the Earth's temperature during 1837−2020 can be characterized by sinusoidal-like cycles of ~60 years, with a peak-to-trough amplitude of approximately 0.25–0.3 °C; (2) These cycles show a general declining trend from 1837 to 2050, implying that planetary orbits have a cooling effect on the Earth over more than two centuries; (3) Planetary orbits generally warmed up the Earth during 1840–1870, 1903–1945, and 1980–present by ~ 0.27, 0.19, and 0.14 °C, respectively. On the other hand, they had an overall cooling effect during 1870−1903 and 1945−1980 of approximately 0.33 and 0.29 °C, respectively; (4) Planetary orbits will generally cause the global temperature to increase by ~0.13 °C from 2020 to 2027 and decrease by ~0.25 °C from 2027 to 2050; and (5) The warming effect of CO_2 was gradual (almost linear) before ~1950, but it became rapid (almost exponential) after ~1950.

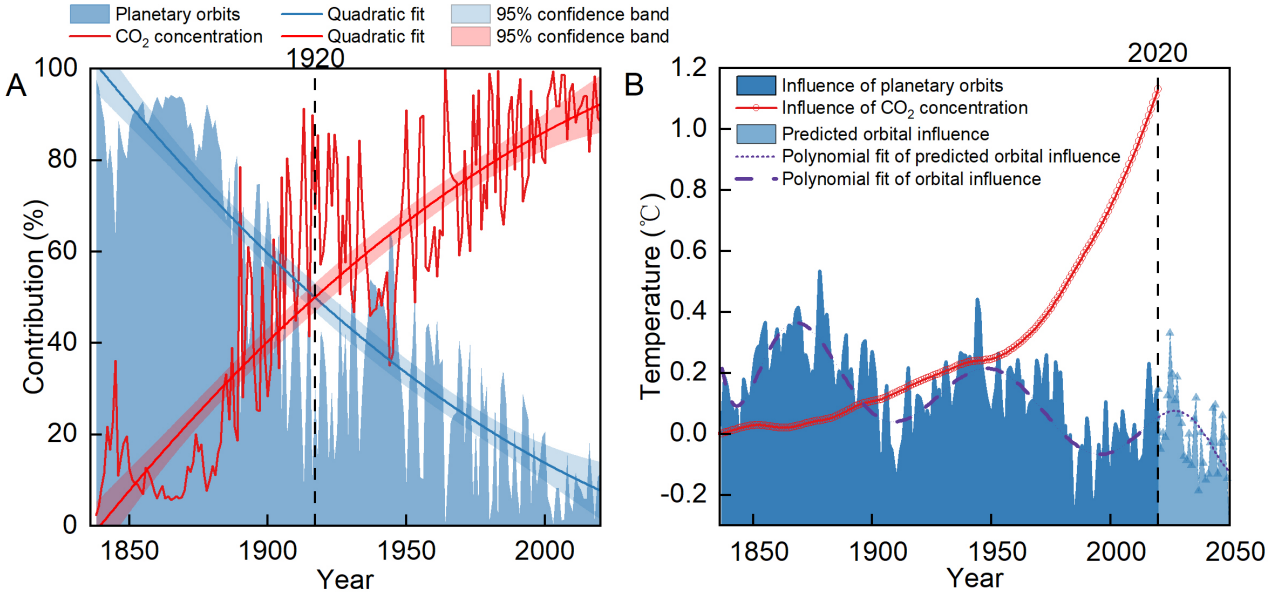

Fig. 3. (**A**) The contribution of planetary orbits and CO_2 concentrations to Earth's temperature changes from 1837 to 2020 using 1836 as the benchmark. (**B**) Earth's temperature changes due to changes in planetary orbits and CO_2 concentrations from 1837 to 2020 and values of Earth's

temperature change from 2020 to 2050 obtained using the forecast model developed based on the LSTM and spectral domain methods.

It should be noted that in the process of quantifying the effects of different planetary orbits (i.e., Earth's rotation, lunar revolution, Earth's revolution and the common motion of the seven major planets) on changes in Earth's temperature, our model assumes that the effect of total solar radiative output on Earth's temperature remains constant for two consecutive hours, two consecutive days, two consecutive sidereal months and two consecutive years, which can help us remove the effect of solar forcing change on Earth's temperature change. Although the lack of successive accurate measurements of solar radiation in the early days will inevitably lead to partial inclusion of solar-induced temperature changes in our estimates, variation of solar radiation is at most 0.5% and ~0.1% in a few days and a few years, respectively, so their effects on successive changes in Earth's temperature are very small [40]. Therefore, this has little effect on our model, and we take the average of these consecutive estimates as the final estimate, which further reduces the error of the model estimate.

Furthermore, according to the CO_2-induced temperature change trend in Fig. 3B, if human beings do not take appropriate measures, the Earth's temperature will rise by approximately 0.43 ℃ (based on the impact of CO_2 on the Earth's temperature from 1837 to 2020) or even by 1.2 ℃ (based on the impact of CO_2 on the Earth's temperature from 1950 to 2020) over the next 30 years. In addition, temperature projections by the end of the 21st century under four RCPs (i.e., RCP2.6, RCP4.5, RCP6.0 and RCP8.5) and five illustrative scenarios (i.e., SSP1-1.9, SSP1-2.6, SSP2-4.5, SSP3-7.0 and SSP5-8.5) show that global surface temperature will continue to increase until at least mid-century [12,13]. Among them, the warming rate is the largest under the highest emission scenario (i.e., RCP8.5 and SSP5-8.5), which is projected to warm at a rate greater than 0.3 °C per decade in 2020-2100 [12,13,41]. Even under the very low emissions scenario considered (RCP2.6 and SSP1-1.9), a further warming of about 0.15 °C per decade would be expected over the next three decades (2020-2050) [12,13,42]. While our results suggest that the planet's orbit will trigger a maximum cooling of the Earth by approximately 0.32 °C over the next 30 years, it will not be enough to reverse the warming trend. This research and analysis can help us more systematically understand Earth's temperature change and develop carbon reduction measures, thereby helping humanity effectively control temperature change to below 2 °C or even 1.5 °C in the 21st century.

Main References

1 Blöschl, G. *et al.* Changing climate shifts timing of European floods. *Science* **357**, 588-590, doi:10.1126/science.aan2506 (2017).

2 Carleton Tamma, A. & Hsiang Solomon, M. Social and economic impacts of climate. *Science* **353**, aad9837, doi:10.1126/science.aad9837 (2016).

3 Kump, L. Climate change and marine mass extinction. *Science* **362**, 1113-1114, doi:10.1126/science.aav736 (2018).

4 Laufkötter, C., Zscheischler, J. & Frölicher Thomas, L. High-impact marine heatwaves attributable to human-induced global warming. *Science* **369**, 1621-1625, doi:10.1126/science.aba0690 (2020).

5 Fletcher Sara, E. M. & Schaefer, H. Rising methane: A new climate challenge. *Science* **364**, 932-933, doi:10.1126/science.aax1828 (2019).

6 Lacis Andrew, A., Schmidt Gavin, A., Rind, D. & Ruedy Reto, A. Atmospheric CO2: Principal Control Knob Governing Earth's Temperature. *Science* **330**, 356-359, doi:10.1126/science.1190653 (2010).
7 Lashof, D. A. & Ahuja, D. R. Relative contributions of greenhouse gas emissions to global warming. *Nature* **344**, 529-531, doi:10.1038/344529a0 (1990).
8 Levitus, S. *et al.* Anthropogenic Warming of Earth's Climate System. *Science* **292**, 267-270, doi:10.1126/science.1058154 (2001).
9 IPCC. Climate Change: The IPCC Scientific Assessment Contribution of Working Group I to the First Assessment Report of the Intergovernmental Panel on Climate Change. (Cambridge University Press, 1990).
10 IPCC. Climate Change 1995: The Science of Climate Change, the Contribution of Working Group 1 to the Second Assessment Report of the Intergovernmental Panel on Climate Change. (Cambridge University Press, 1996).
11 IPCC. Summary for Policymakers. In: Climate Change 2007: The Physical Science Basis. Contribution of Working Group I to the Fourth Assessment Report of the Intergovernmental Panel on Climate Change. (Cambridge University Press, 2007).
12 IPCC. Summary for Policymakers. In: Climate Change 2013: The Physical Science Basis. Contribution of Working Group I to the Fifth Assessment Report of the Intergovernmental Panel on Climate Change. (Cambridge University Press, 2013).
13 IPCC. Summary for Policymakers. In: Climate Change 2021: The Physical Science Basis. Contribution of Working Group I to the Sixth Assessment Report of the Intergovernmental Panel on Climate Change. (Cambridge University Press, 2021).
14 IPCC. Climate Change 2001: The Scientific Basis. Contribution of Working Group I to the Third Assessment Report of the Intergovernmental Panel on Climate Change. (Cambridge University Press,2001).
15 Bradley, R. S. & Jonest, P. D. 'Little Ice Age' summer temperature variations: their nature and relevance to recent global warming trends. *The Holocene* **3**, 367-376, doi:10.1177/095968369300300409 (1993).
16 Scafetta, N. Reconstruction of the Interannual to Millennial Scale Patterns of the Global Surface Temperature. *Atmosphere* **12**, doi:10.3390/atmos12020147 (2021).
17 Briffa, K. R. *et al.* A 1,400-year tree-ring record of summer temperatures in Fennoscandia. *Nature* **346**, 434-439, doi:10.1038/346434a0 (1990).
18 Brook, E. J. & Buizert, C. Antarctic and global climate history viewed from ice cores. *Nature* **558**, 200-208, doi:10.1038/s41586-018-0172-5 (2018).
19 Guiot, J., Pons, A., de Beaulieu, J. L. & Reille, M. A 140,000-year continental climate reconstruction from two European pollen records. *Nature* **338**, 309-313, doi:10.1038/338309a0 (1989).
20 Klyashtorin, L. B., Borisov, V. & Lyubushin, A. Cyclic changes of climate and major commercial stocks of the Barents Sea. *Marine Biology Research* **5**, 4-17, doi:10.1080/17451000802512283 (2009).
21 Marsicek, J., Shuman, B. N., Bartlein, P. J., Shafer, S. L. & Brewer, S. Reconciling divergent trends and millennial variations in Holocene temperatures. *Nature* **554**, 92-96, doi:10.1038/nature25464 (2018).
22 Raymo, M. E., Ganley, K., Carter, S., Oppo, D. W. & McManus, J. Millennial-scale climate instability during the early Pleistocene epoch. *Nature* **392**, 699-702, doi:10.1038/33658 (1998).

23 Croll, J. XIII. On the physical cause of the change of climate during geological epochs. *The London, Edinburgh, and Dublin Philosophical Magazine and Journal of Science* **28**, 121-137, doi:10.1080/14786446408643733 (1864).
24 Gribbin, J. Planetary Alignments, Solar Activity and Climatic Change. *Nature* **246**, 453-454, doi:10.1038/246453a0 (1973).
25 Tardif, D. *et al.* Orbital variations as a major driver of climate and biome distribution during the greenhouse to icehouse transition. *Science Advances* **7**, eabh2819, doi:10.1126/sciadv.abh2819.
26 Zachos, J. C., Flower, B. P. & Paul, H. Orbitally paced climate oscillations across the Oligocene/Miocene boundary. *Nature* **388**, 567-570, doi:10.1038/41528 (1997).
27 Milankovictch, M. *Canon of insolation and the ice-age problem (Kanon der Erdbestrahlung und seine Anwendung auf das Eiszeitenproblem) Belgrade, 1941*. (1969).
28 Scafetta, N. Empirical evidence for a celestial origin of the climate oscillations and its implications. *Journal of Atmospheric and Solar-Terrestrial Physics* **72**, 951-970, doi: 10.1016/j.jastp.2010.04.015 (2010).
29 Balling Robert, C. & Cerveny Randall, S. Influence of Lunar Phase on Daily Global Temperatures. *Science* **267**, 1481-1483, doi:10.1126/science.267.5203.1481 (1995).
30 Condon, J. J. & Schmidt, R. R. Planetary tides and sunspot cycles. *Solar Physics* **42**, 529-532, doi:10.1007/BF00149930 (1975).
31 Hays, J. D., Imbrie, J. & Shackleton, N. J. Variations in the Earth's Orbit: Pacemaker of the Ice Ages. *Science* **194**, 1121-1132, doi:10.1126/science.194.4270.1121 (1976).
32 Friis-Christensen, E. & Lassen, K. Length of the Solar Cycle: An Indicator of Solar Activity Closely Associated with Climate. *Science* **254**, 698, doi:10.1126/science.254.5032.698 (1991).
33 Lassen, K. & Friis-Christensen, E. Variability of the solar cycle length during the past five centuries and the apparent association with terrestrial climate. *Journal of Atmospheric and Terrestrial Physics* **57**, 835-845, doi:10.1016/0021-9169(94)00088-6 (1995).
34 Scafetta, N. High resolution coherence analysis between planetary and climate oscillations. *Advances in Space Research* **57**, 2121-2135, doi:10.1016/j.asr.2016.02.029 (2016).
35 Scafetta, N., Milani, F., Bianchini, A. & Ortolani, S. On the astronomical origin of the Hallstatt oscillation found in radiocarbon and climate records throughout the Holocene. *Earth-Science Reviews* **162**, 24-43, doi:10.1016/j.earscirev.2016.09.004 (2016).
36 Wang, Z., Wu, D., Song, X., Chen, X. & Nicholls, S. Sun-Moon gravitation-induced wave characteristics and climate variation. *Journal of Geophysical Research: Atmospheres* **117**, doi:10.1029/2011JD016967 (2012).
37 Berger, A., Loutre, M. F. & Laskar, J. Stability of the Astronomical Frequencies Over the Earth's History for Paleoclimate Studies. *Science* **255**, 560-566, doi:10.1126/science.255.5044.560 (1992).
38 Zhang, S. *et al.* Orbital forcing of climate 1.4 billion years ago. *Proceedings of the National Academy of Sciences* **112**, E1406-E1413, doi:10.1073/pnas.1502239112 (2015).
39 Zhang, X. *et al.* Direct astronomical influence on abrupt climate variability. *Nature Geoscience* **14**, 819-826, doi:10.1038/s41561-021-00846-6 (2021).
40 Eddy, J. A., Gilliland, R. L. & Hoyt, D. V. Changes in the solar constant and climatic effects. *Nature* **300**, 689-693, doi:10.1038/300689a0 (1982).
41 Rogelj, J., Meinshausen, M. & Knutti, R. Global warming under old and new scenarios using IPCC climate sensitivity range estimates. *Nature Climate Change* **2**, 248-253, doi:10.1038/nclimate1385 (2012).

42 Rogelj, J. *et al.* Differences between carbon budget estimates unravelled. *Nature Climate Change* **6**, 245-252, doi:10.1038/nclimate2868 (2016).

Methods:

1) Quantifying the intra-annual contribution of planetary orbits to changes in Earth's temperature

1.1) Model specification

The temporal variations in Earth's temperature are mainly driven by the Earth's revolution and rotation. The temporal variations in Earth's temperature also differ from cycle to cycle (including diurnal and annual cycles) due to the changes in the position of the Moon and other planets relative to the Earth. To quantify the contribution of different planetary orbits to the Earth's temperature, we developed a function describing the influence of different orbits on the Earth's temperature over time. We performed a Fourier series analysis of the hourly temperature records, which showed that 1) the amplitude to range ratio (A/R) of the first few harmonic terms is nearly constant over the entire annual range, and 2) the sum of A/R for the 24'-h and 365'-d terms exceeds 0.87.

It is evident that the variations in the Earth's temperature during a year are mainly dependent on the rotation and revolution of the Earth. The departure from 0.87 is indicative of the influence of other factors on the variation in Earth's temperature. This suggests that (1) a unit curve, $X(t)$, can be used to derive the annual variation in temperature, whose duration depends on the temporal variability of the Earth's revolution, and (2) the annual cycle unit curve ($X(t)$) can consist of a series of functions describing the effect of different orbits on the Earth's temperature perturbations.

$$X(t) = f_1(t) + f_2(t) + f_3(t) + Z(t) \quad (1)$$

where $X(t)$ represents the transformed influence of all planetary orbits on the change in Earth's temperature at time *t*. The transformed influence is the influence value divided by the range, and the ranges in the section refer to the difference of the maximum and minimum hourly temperatures in a year, $T_{max} - T_{min}$, unless otherwise indicated. $X(t)$ was then determined by the summation of four functions, i.e., f_1, f_2, f_3, and Z. $f_1(t)$, $f_2(t)$ and $f_3(t)$ represent the transformed influence of Earth's rotation, lunar revolution and Earth's revolution on Earth's temperature changes at time *t*, respectively. $Z(t)$ denotes the transformed effect of the orbits of the other seven planets (namely, Mercury, Mars, Jupitar, Saturn, Neptune, Venus and Uranus) in the solar system on the change in the Earth's temperature at time *t*.

$f_1(t)$ and $f_3(t)$ can be obtained by dividing the influence of Earth's rotation and revolution on Earth's temperature on shorter time scales within the annual temperature cycle by the range. The motion of the Earth (i.e., rotation and revolution) and its impact on the Earth's temperature are all periodic. The Fourier series analysis of hourly temperature data revealed that the amplitudes of the harmonic terms corresponding to the rotation and revolution period times are nearly constant. Thus, functions composed of harmonic terms can be used to describe the effects of Earth's rotation and Earth's revolution on changes in Earth's temperature during a year.

$$f_1(t) = \frac{E_m^n}{T_{max}-T_{min}} \cos\left[\frac{2\pi}{\omega_1}(t_l - h_m^n)\right] + \frac{r_m^n}{T_{max}-T_{min}} \quad (2)$$

$$f_3(t) = \frac{A_3}{T_{max}-T_{min}} \cos\left[\frac{2\pi}{\omega_3}(t - c)\right] + \frac{q}{T_{max}-T_{min}} \quad (3)$$

where t_l represents the t_l-th hour of the *m*th day of the *n*th sidereal month, and *t* is the hour of the year. E_m^n and A_3 are the harmonic amplitudes (which can be obtained by a Fourier series analysis), r_m^n and q are the exponential terms, and h_m^n and c are the optional phase shifts for $f_1(t)$ and $f_3(t)$, respectively. To improve the convergence of $f_1(t)$ and $f_3(t)$, *a priori* knowledge about the hours

of their motion is needed. The widths ω_1 and ω_3 in the cosine terms are determined by the hours in which they complete their periodic motions.

Given the physical continuity of Earth's temperature, the influence functions of Earth's rotation and revolution on the temperature (i.e., $f_1(t)$ and $f_3(t)$) are presumed to be continuous in all instances, including the junction time between two diurnal cycles (t_{l^0}) and the junction time between two consecutive years (t_0). Herein, we evaluate the continuity of the influence functions of the Earth's rotation ($f_1(t)$) and Earth's revolution ($f_3(t)$). $f_1(t)$ for Days m and m+1 can be expressed as:

$$f_1{}^m(t) = \frac{E_m^n}{T_{max}-T_{min}} \cos\left[\frac{2\pi}{\omega_1}(t_l - h_m^n)\right] + \frac{r_m^n}{T_{max}-T_{min}} \quad (4)$$

$$f_1{}^{m+1}(t) = \frac{E_{m+1}^n}{T_{max}-T_{min}} \cos\left[\frac{2\pi}{\omega_1}(t_l - h_{m+1}^n)\right] + \frac{r_{m+1}^n}{T_{max}-T_{min}} \quad (5)$$

For $f_1(t)$ to be continuous at the junction time between two diurnal cycles (t_{l^0}), the following two constraints should be fulfilled:

$$f_1{}^m(t)|_{t=t_{l^0}} = f_1{}^{m+1}(t)|_{t=t_{l^0}} \quad (6)$$

$$\left(\frac{\partial f_1{}^m(t)}{\partial t}\right)|_{t=t_{l^0}} = \left(\frac{\partial f_1{}^{m+1}(t)}{\partial t}\right)|_{t=t_{l^0}} \quad (7)$$

Substituting Equations (4) and (5) into (6) and their derivatives into (7) leads to:

$$E_{m+1}^n = \frac{E_m^n \sin\left[\frac{2\pi}{\omega_1}(t_{l^0}-h_m^n)\right]}{\sin\left[\frac{2\pi}{\omega_1}(t_{l^0}-h_{m+1}^n)\right]} \quad (8)$$

$$r_{m+1}^n = E_m^n \cos\left[\frac{2\pi}{\omega_1}(t_{l^0} - h_m^n)\right] + r_m^n - E_{m+1}^n \cos\left[\frac{2\pi}{\omega_1}(t_{l^0} - h_{m+1}^n)\right] \quad (9)$$

Equation (8) allows us to obtain E_{m+1}^n in terms of E_m^n. Similarly, Equation (9) relates r_{m+1}^n to r_m^n. A multiday continuous $f_1(t)$ model can be obtained by substituting (8) and (9) into (5). The total number of free parameters in the function $f_1(t)$ for Day m ($m \geq 2$) is m+1 (i.e., r for the first day and h_1^n to h_m^n), and these free parameters are estimated with the Levenberg–Marquardt minimization algorithm with a universal global optimization scheme [43]. E and r for each day (except the first day) are calculated from (8) and (9), respectively.

Analogously, the function $f_3(t)$ must be continuous in all instances, including the junction time between two consecutive years (t_0). $f_3(t)$ for years i and i+1 can be expressed as:

$$f_3{}^i(t) = \frac{A_3{}^i}{T^i{}_{max}-T^i{}_{min}} \cos\left[\frac{2\pi}{\omega_3{}^i}\left(t - c^i\right)\right] + \frac{q^i}{T^i{}_{max}-T^i{}_{min}} \quad (10)$$

$$f_3{}^{i+1}(t) = \frac{A_3{}^{i+1}}{T^{i+1}{}_{max}-T^{i+1}{}_{min}} \cos\left[\frac{2\pi}{\omega_3{}^{i+1}}\left(t - c^{i+1}\right)\right] + \frac{q^{i+1}}{T^{i+1}{}_{max}-T^{i+1}{}_{min}} \quad (11)$$

For $f_3(t)$ to be continuous at the junction time between two annual cycles (t_0), the following two constraints should be fulfilled:

$$f_3{}^i(t)|_{t=t_0} = f_3{}^{i+1}(t)|_{t=t_0} \quad (12)$$

$$\left(\frac{\partial f_3{}^i(t)}{\partial t}\right)|_{t=t_0} = \left(\frac{\partial f_3{}^{i+1}(t)}{\partial t}\right)|_{t=t_0} \quad (13)$$

Substituting Equations (10) and (11) into (12) and their derivatives into (13) leads to:

$$A_3{}^{i+1} = \frac{A_3{}^i \sin\left[\frac{2\pi}{\omega_3{}^i}(t_0-c^i)\right]}{\sin\left[\frac{2\pi}{\omega_3{}^{i+1}}(t_0-c^{i+1})\right]} \quad (14)$$

$$q^{i+1} = {A_3}^{i}\cos\left[\frac{2\pi}{{\omega_3}^{i}}\left(t_0 - c^{i}\right)\right] + q^{i} - {A_3}^{i+1}\cos\left[\frac{2\pi}{{\omega_3}^{i+1}}\left(t_0 - c^{i+1}\right)\right] \quad (15)$$

A multiyear continuous $f_3(t)$ model can be obtained by substituting (14) and (15) into (11). The total number of free parameters in the function $f_3(t)$ for year i ($i \geq 2$) is i+1 (i.e., q for the first year and c^1 to c^i), and these free parameters are estimated with the Levenberg–Marquardt minimization algorithm with a universal global optimization scheme [43]. A_3 and q for each year (except the first year) are calculated from (14) and (15), respectively.

$f_2(t)$ is obtained by dividing the influence of the lunar revolution on the Earth's temperature by the range. In each sidereal month, the Moon affects the Earth's temperature by different physical processes, namely, the magnetic force, lunar phase changes, orbital oscillations, reflections, and infrared emissions from the Moon's surface. It is worth mentioning that these processes have different cycles. In addition, the Earth-Moon system moves around the Sun, while the Moon orbits the Earth. Such a complex system induces different feedbacks in the Earth system. Therefore, the influence of the Moon's orbit on the Earth's temperature is irregular and varies among revolution periods, which makes it extremely difficult to find an appropriate function to express the influence of the Moon on the Earth's temperature.

As explained in Supplementary Sections 1.2 and 1.3, the temperature changes in two successive days are mainly driven by the revolution of the Earth and Moon. Therefore, the temperature difference (D2) between two subsequent days can be inferred by taking the derivative of the sum of the functions that describe the influence of the revolution of the Earth and Moon on the Earth's temperature change, i.e., $D2 = \frac{d\,(f2+f3)}{dt}$. It is evident that the influence of the Moon's orbit on the Earth's temperature (y) can be calculated by subtracting the influence of Earth's revolution (see Equation 3) from the antiderivative function (F) of $D2$ as follows:

$$F(t) = \frac{d}{dt}\left[\int\left(f_2(t) + f_3(t)\right)dt\right] + C = \int D2(t)dt + C \quad (16)$$

$$y_n(t_s) = F_n(t_s) - [A_3\cos\left[\frac{2\pi}{\omega_3}(t - c)\right] + q] \quad (17)$$

where C is a constant, n represents the n-th sidereal month, and t_s represents the t_s-th hour of the n-th sidereal month.

The function $f_2(t)$ for the n-th sidereal month of the i-th year is calculated by dividing the influence of the Moon's orbit on the Earth's temperature (y) by the range:

$$f_2(t)_n^i = \frac{y_n(t_s)}{T_{max} - T_{min}} \quad (18)$$

$Z(t)$ can be calculated by dividing the influence of the abovementioned seven planets in the solar system on Earth's temperature during a year by the range. The influence of the seven planets on Earth's temperature can be determined by a physical function that depends on the orbits of the planets and their positions. However, it is difficult to build such a function because the physical mechanisms that relate the motion of a single planet to Earth's temperature still need to be further investigated, even though the movement of each planet can be strictly calculated. In addition, the lack of sufficient data and the complexity of the physical processes linking the Earth's temperature to the entire planetary system limit the determination of this function [28].

On the other hand, the impacts of the Earth's revolution, lunar revolution and Earth's rotation on Earth's temperature occur periodically on a subannual timescale, and their cumulative effects on Earth's temperature changes are roughly similar in each cycle. The effect of solar forcing and the

change in CO_2 concentration in two consecutive years on Earth's temperature is negligible, and seven planetary orbits mainly affect Earth's temperature on interannual or even longer time scales [27,28,40]. Hence, it is hypothesized that changes in the Earth's temperature between two consecutive years arise from the abovementioned seven planets in the solar system. Having said that, $Z(t)$ for year i can be calculated by normalizing the difference of Earth's temperatures in that year and the previous year by the difference of the maximum and minimum hourly temperatures in that year as follows:

$$Z(t)^i = \frac{\mathrm{MT}^i - \mathrm{MT}^{i-1}}{({T^i}_{max} - {T^i}_{min})} \tag{19}$$

where MT^i and MT^{i-1} are the mean temperatures of the Earth in years i and $i-1$, respectively. ${T^i}_{max}$ and ${T^i}_{min}$ are the maximum and minimum hourly temperatures of year i, respectively.

This study defines that the contribution of different orbits to the annual Earth's temperature perturbations is equal to the annual temperature variation caused by different orbits divided by the maximum annual temperature variation. Therefore, the contributions of Earth's rotation and revolution to the intra-annual fluctuation of Earth's temperature are calculated by dividing the magnitude of intra-annual temperature variations caused by each of them by the highest annual temperature change (see Eqs. 20–21).

$$g_1^i = \frac{\frac{1}{h}\sum_{n=1}^{k}\sum_{m=1}^{j}(E_m^n)}{{T^i}_{max} - {T^i}_{min}} \tag{20}$$

$$g_3^i = \frac{{A_3}^i}{{T^i}_{max} - {T^i}_{min}} \tag{21}$$

where g_1^i and g_3^i are the contributions of Earth's rotation and revolution to the annual Earth temperature variation in year *i*, respectively. *k* is the number of sidereal months in year *i*, *j* is the number of days in the *n*-th sidereal month, and *h* is the total number of days in year *i*.

The normalized intra-annual temperature variation caused by lunar revolution is given by

$$g_2^i = \frac{\frac{1}{k}\sum_{n=1}^{k}(y_{max}^n - y_{min}^n)}{{ET^i}_{max} - {ET^i}_{min}} \tag{22}$$

where g_2^i is the contribution of the lunar revolution to the annual Earth's temperature variation in year i and k is the number of sidereal months in year i. y_{max}^n and y_{min}^n are the maximum and minimum y (the influence of the Moon's orbit on the Earth's temperature) in the sidereal month n, respectively.

The contribution (g_z) of the orbits of other planets in the solar system to the changes in the Earth's temperature during a year is numerically equal to the transformed influence $\big(Z(t)\big)$.

$$g_z^i = Z(t)^i \tag{23}$$

where g_z^i is the contribution in year i of the orbits of other planets in the solar system to the change in the Earth's temperature during a year.

1.2) Combination of the model from Section 1.1 and historical temperature data

$f_1(t)$ quantifies the influence of Earth's rotation on its intra-annual temperature variation. Building on Section 1.1 of the Supplementary Materials, the quasi-sinusoidal diurnal variation in Earth's temperature (Supplementary Fig. S1) is mainly due to its rotation. We calculated the temperature difference (D1) of two consecutive hours for each day from 1979 to 2020. A remarkable agreement is found between the D1 values of two consecutive days. For example, the D1 values for January 1 and 2 from 1979-2020 are shown in Extended Data Fig. 1. These results indicate that the variation

in D1 is mainly determined by the rotation of the Earth. Therefore, the changes in D1 can be used to quantify the impact of Earth's rotation on the global temperature in consecutive hours, which can be inferred by taking the derivative of the function $f_1(t)$. The derivative of $f_1(t)$ is fitted to the time series of D1 by using the Levenberg–Marquardt scheme to obtain its unknown parameters.

$f_2(t)$ quantifies the influence of the lunar revolution on the intra-annual Earth's temperature variations. The changes in CO_2 concentration for two consecutive days have almost no effect on the Earth's temperature. Thus, we can determine the change in Earth's temperature over two consecutive days (due the motion of the Moon) by using Equations (16) − (18). To eliminate the impact of large variations in CO_2 concentration in two successive days on temperature, we utilized only D2 values for days in which the CO_2 concentration was relatively stable.

The changes in the Earth's temperature during each year can be attributed to the variations in solar radiation absorbed by the land and the speed of the Earth's rotation, which are induced by the Earth's revolution to a certain extent (Supplementary Section 1.3). Thus, the intra-annual temperature change can be used to quantify the contribution of the Earth's revolution to the temperature. Additionally, the results of the Supplementary Materials (Section 1.2) show that the influence of the Moon's movement on the intra-annual temperature changes is not negligible. Since the Moon orbits the Earth once per sidereal month, we can reasonably assume that the Moon's effect on Earth's temperature changes is approximately similar in each month. The sidereal monthly Earth's temperature averaged over the study period (1979−2020) is compared with the corresponding solar declination (Extended Data Fig. 2A). Extended Data Fig. 2B shows the scatterplot of the mean sidereal monthly Earth's temperature versus the corresponding solar declination for each sidereal month during the study period. It was found that the solar declination had a stronger correlation with the mean sidereal monthly temperature (with an R^2 of 0.928) than the daily temperature (with an R^2 of 0.786 (Supplementary Fig. S5)). This further suggest that the variation in the mean sidereal monthly temperature is driven by Earth's revolution.

The CO_2 concentration in two successive sidereal months is almost constant. Therefore, the temperature difference of consecutive sidereal months (D3) can be used to quantify the impact of the Earth's revolution on temperature. To further exclude the influence of CO_2 on temperature, we used only the D3 values of sidereal months with stabilized CO_2 concentrations. The function $f_3(t)$ quantifies the influence of Earth's revolution on the intra-annual variations in Earth's temperature, whereas D3 can be inferred by taking the derivative of the function $f_3(t)$. It is evident that the derivative of $f_3(t)$ can be fitted to the time series of D3 by using the Levenberg–Marquardt scheme to obtain its unknown parameters.

$Z(t)$ quantifies the influence of all planets in the solar system on the intra-annual variations in Earth's temperature. To eliminate the influence of CO_2 changes on variations in the Earth's temperature, we considered the temperature difference of two successive years in which the CO_2 concentration was almost unchanged.

2) Quantifying the contribution of planetary orbits to changes in Earth's temperature on an interannual scale

In this study, the variation in Earth's temperature at various time intervals can be defined by Equation 24:

$$T_{i+s} - T_i = P_{i+s,i} + V_{i+s,i} \tag{24}$$

where $T_{i+s} - T_i$ is the temperature difference between years *i*+*s* and *i*, and $P_{i+s,i}$ and $V_{i+s,i}$ are the effects of planetary orbits and greenhouse gases on changes in Earth's temperature between years *i*+*s* and *i*, respectively.

Ample physical evidence shows that CO_2 is the most important gas for controlling Earth's temperature [6]. On the other hand, it is difficult to obtain the records of other greenhouse gases before 1979. Hence, we equate Earth's temperature change caused by other greenhouses with the effect of CO_2. Equation 24 can be rewritten as 25 based on the near-linear relationship between CO_2 and Earth's temperature change [13].

$$T_{i+s} - T_i = P_{i+s,i} + dV_{i+s,i} \times v \tag{25}$$

where $dV_{i+s,i}$ is the difference in CO_2 concentration between years *i*+*s* and *i*. v is the value of the Earth's temperature change caused by 1 ppm CO_2.

If the effect of a unit change in CO_2 concentration (v) on the Earth's temperature is obtained, we can accurately quantify the effect of planetary orbits on Earth's temperature change using Equation 25. The estimates from Equation 19 show that the effect of planetary orbits (Z) on the Earth's temperature in different years is small and irregular, ranging from -0.3 °C to 0.26 °C (Extended Data Fig.3). Therefore, it is assumed that the effects of the planet's orbit on the Earth's temperature at various time intervals ($P_{i+s,i}$) can be equal to the mean ($\bar{Z}$) derived from Z during the study period (1836−2020).

$$\bar{Z} = \frac{\sum_{i=1}^{n} |Z_i|}{n} \tag{26}$$

$$P_{i+s,i} = \bar{Z} \tag{27}$$

where Z_i denotes the effect of planetary orbits on Earth's temperature change between years *i*+1 and *i*, which can be obtained from Equation 19. n is the number of Z_i. Then, we can calculate the effect ($v_{i+s,i}$) of 1 ppm CO_2 on temperature at various time intervals by Equation 28.

$$v_{i+s,i} = \frac{T_{i+s} - T_i - \bar{Z}}{dV_{i+s,i}} \quad (s \in [2,184], i \in [1836,2020 - s]) \tag{28}$$

To further improve the estimation accuracy, the mean ($\bar{v}$) of $v_{i+s,i}$ is utilized to approximate the effect (v) of a 1 ppm increase in CO_2 concentration on the global temperature change. In this way, we obtain the effect of a unit change in CO_2 concentration on the Earth's temperature, and then the effect of planetary orbits on the Earth's temperature ($P_{i+s,i}$) between years *i*+*s* and *i* can be obtained via

$$P_{i+s,i} = T_{i+s} - T_i - dV_{i+s,i} \times \bar{v} \tag{29}$$

where $\bar{v}$ is the optimal approximation of the real effect of 1 ppm CO_2 on global temperature change, which is obtained by calculating the average value of all $v_{i+s,i}$.

Finally, the contribution of planetary orbitals (I_o) and CO_2 (I_c) to Earth's temperature change can be obtained by

$$I_o = \frac{|P_{i+s,i}|}{|P_{i+s,i}| + dV_{i+s,i} \times \bar{v}} \tag{30}$$

$$I_c = 1 - I_o \quad (31)$$

Based on the mathematical model, we can quantify the contribution of planetary orbits to changes in Earth's temperature on an inter-annual scale. Robustness tests of the model show that the estimates of the effect of planetary orbits on the Earth's temperature changes from our model have high confidence (Supplementary Section 3).

3) Forecasting the effect of planetary orbits on Earth's temperature from 2021−2050

To further predict the effect of planetary orbit changes (P) on the Earth's temperature, we constructed a hybrid forecast model based on long short-term memory (LSTM) [44,45] and spectral domain approaches (i.e., Fast Fourier transform (FFT) and multitaper (MTM) methods) [46], which can overcome the defect that LSTM based on the recursive strategy is very sensitive to the accumulation of errors with the forecasting horizon. The hybrid forecast model uses the P reconstructed by the spectral domain method as the input value of the LSTM method and waveform change feature of the predicted P value (2020-2050) determined by the spectral domain approach to improve the accuracy of LSTM model P forecasting from 2021− 2050.

Extended Data Fig. 4 shows the architecture of the proposed hybrid forecast model based on LSTM and the spectral domain approach. We chose a rolling prediction scheme for the hybrid forecast model. In this scheme, the spectral domain method is initially applied to reconstruct P from 1837 to 2020 and predict P from 2021 to 2050 (Supplementary Section 4). Next, the LSTM model (Supplementary Section 5) is trained to find a pattern between the P at time t_i and the input sequence values of its 53 preceding moments at times t_{i-1}, t_{i-2}, and t_{i-53} (also called a time window) using input sequence $[P, \hat{P}^F, \hat{P}^M]$, where P is the historical P values during 1837−2020, and $\hat{P}^F$ and $\hat{P}^M$ are the P values during 1837−2020 from the FFT and MTM methods, respectively. The future prediction is determined based on the input sequence values in its preceding 53 moments using the identified patterns. Then, their predictions on each horizon are combined to produce the final prediction. The final prediction is used as the latest element of the input sequence to update the sequence, which is further used to predict one more year ahead P. By repeating this process, k-year-ahead predictions can be achieved. Finally, we predicted the P from 2021 to 2050, as shown in Fig. 3B.

Methods References

43 Göttsche, F.-M. & Olesen, F.-S. Modelling the effect of optical thickness on diurnal cycles of land surface temperature. *Remote Sensing of Environment* **113**, 2306-2316, doi:10.1016/j.rse.2009.06.006 (2009).

44 Xiao, C. *et al.* Short and mid-term sea surface temperature prediction using time-series satellite data and LSTM-AdaBoost combination approach. *Remote Sensing of Environment* **233**, 111358, doi:10.1016/j.rse.2019.111358 (2019).

45 Zhong, L., Hu, L. & Zhou, H. Deep learning based multi-temporal crop classification. *Remote Sensing of Environment* **221**, 430-443, doi:10.1016/j.rse.2018.11.032 (2019).

46 Ghil, M. *et al.* ADVANCED SPECTRAL METHODS FOR CLIMATIC TIME SERIES. *Reviews of Geophysics* **40**, 3-1-3-41, doi:10.1029/2000RG000092 (2002).

Acknowledgments: The authors would like to thank the U.S. Department of Energy, Office of Science Biological and Environmental Research (BER), the National Oceanic and Atmospheric Administration Climate Program Office, the NOAA Physical Sciences Laboratory, and the European Centre for Medium-Range Weather Forecasts (ECMWF) for providing the climate

reanalysis data, the Scripps Institution of Oceanography for providing the concentrations of CO_2, the NASA Jet Propulsion Laboratory Developmental Ephemeris for providing the ephemerides for solar-system bodies, and the International Earth Rotation and Reference Systems Service Rapid Service/Prediction Centre for providing the daily length of day data.

Funding: Key Project of Natural Science Foundation of Ningxia Department of Science and Technology (No. 2024AC02032), Fengyun Satellite Application Pilot Program "Development and Application of Fengyun all-weather Land Surface Temperature Spatiotemporal Fusion Dataset" (FY-APP-2022.0205).

Author contributions: KM designed the research. MC and KM developed the methodology. MC, KM, Bateni, JMC, Heggy, JSK and XS contributed to the results analysis and discussion. MC, KM, Bateni, JC and Heggy drafted the manuscript, and all authors revised the manuscript.

Competing interests: The authors declare no competing financial interests.

Data and materials availability: All data used in this study are described in the Supplementary Materials, and all codes are available at https://doi.org/10.5281/zenodo.6969259.

Supplementary Materials

Supplementary Text

Figs. S1 to S10

Tables S1

References

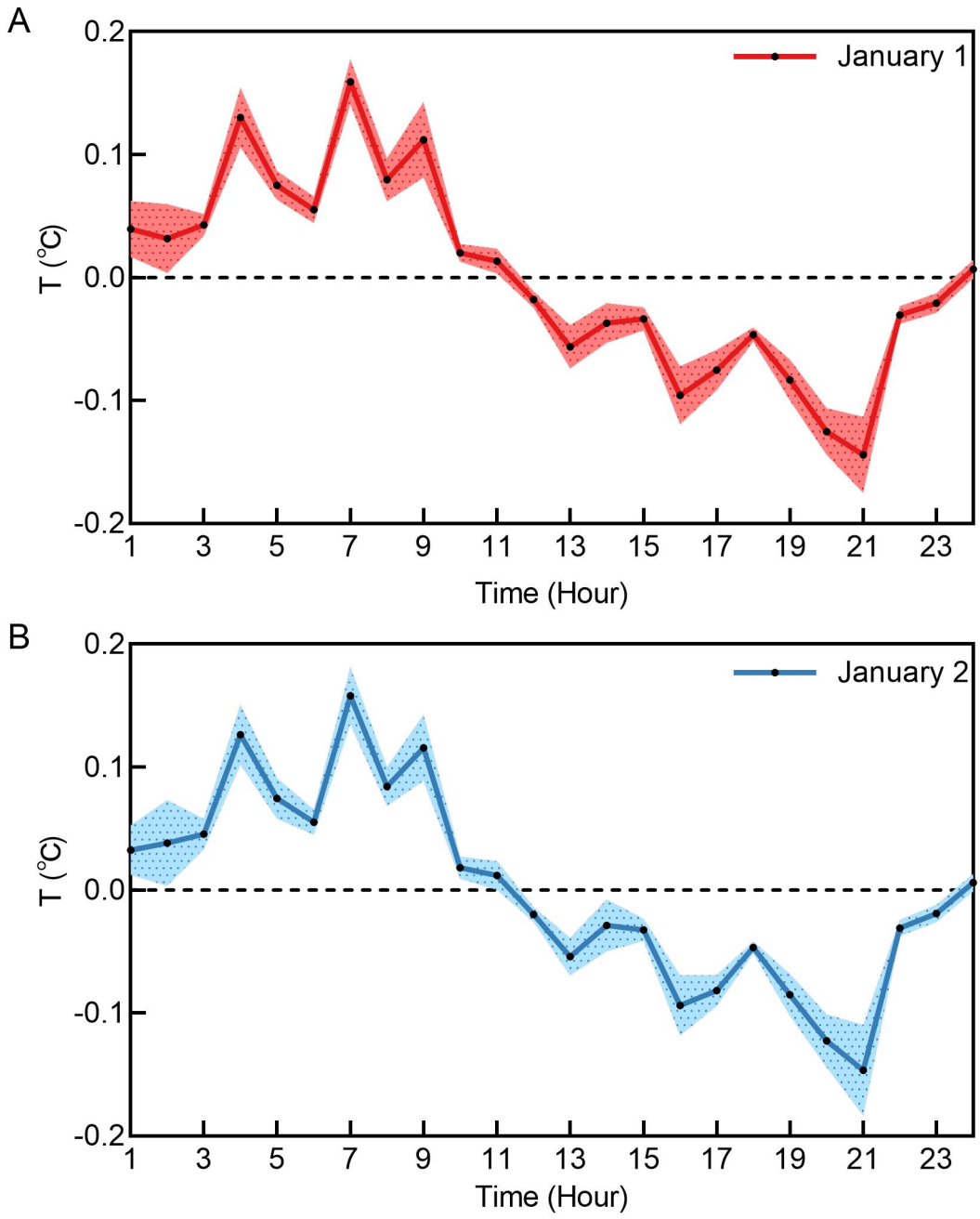

Extended Data Fig. 1.

The temperature difference (D1) of two consecutive hours on January 1 and 2 from 1979−2020. The red and blue bands represent the standard deviation of the temperature difference data of two consecutive hours on January 1 and January 2, respectively, during the study period

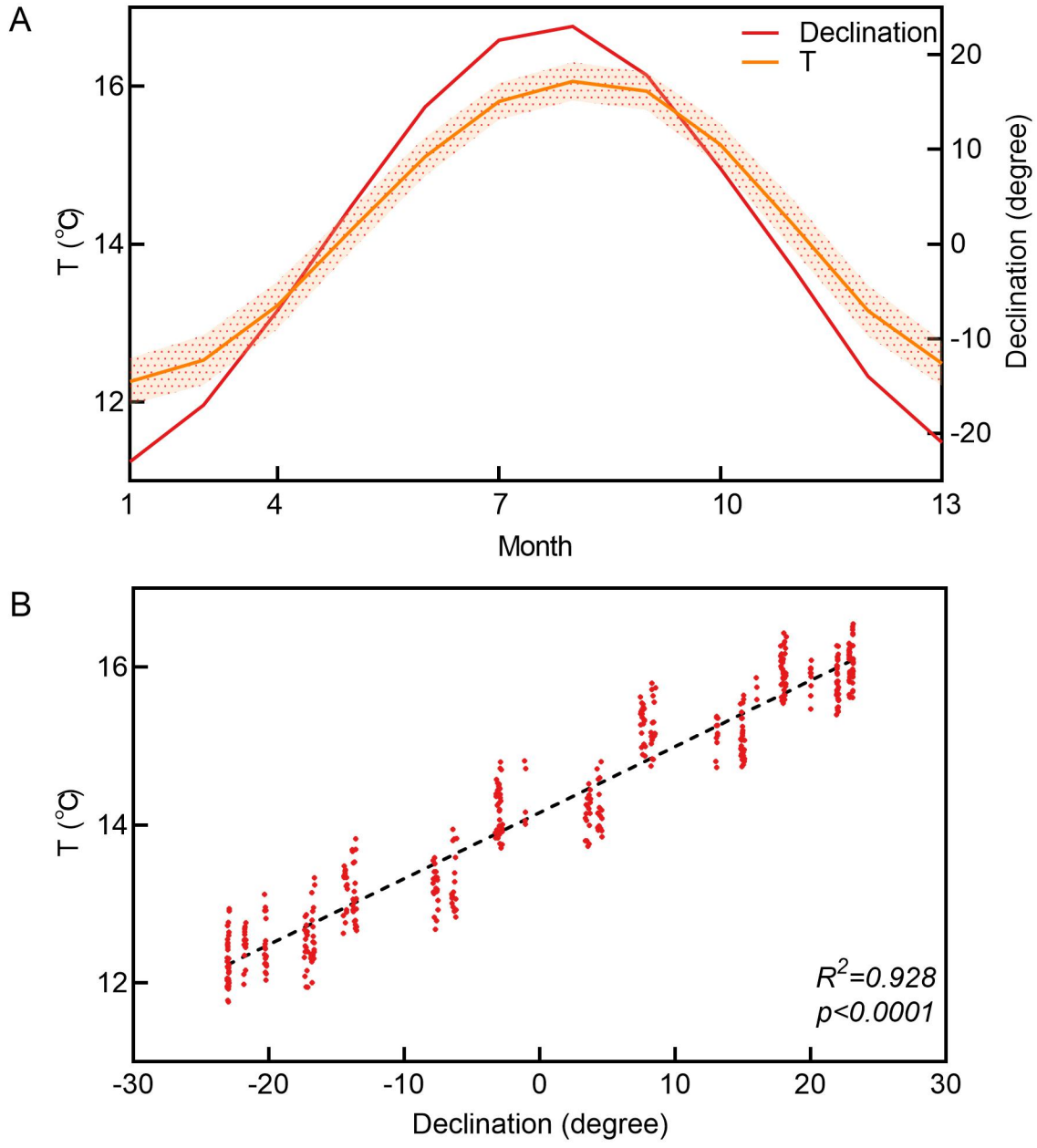

Extended Data Fig. 2.

(**A**) Comparison of sidereal monthly Earth's temperature data averaged over the period 1979−2020 with solar declination. The orange band represents the standard deviation of sidereal monthly Earth's temperature data during the study period. (**B**) Scatterplot of sidereal monthly Earth temperature data versus solar declination during the study period.

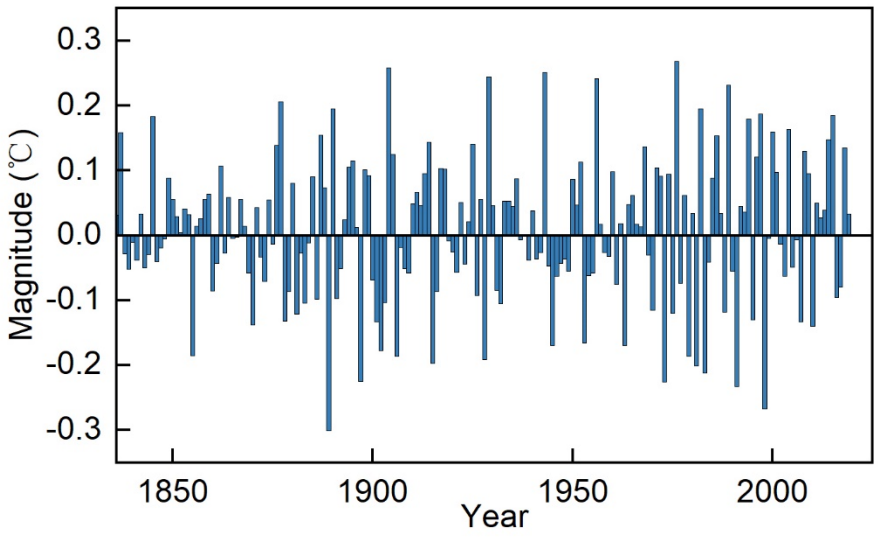

Extended Data Fig. 3.
The effect of planetary orbits on changes in Earth's temperature for two consecutive years.

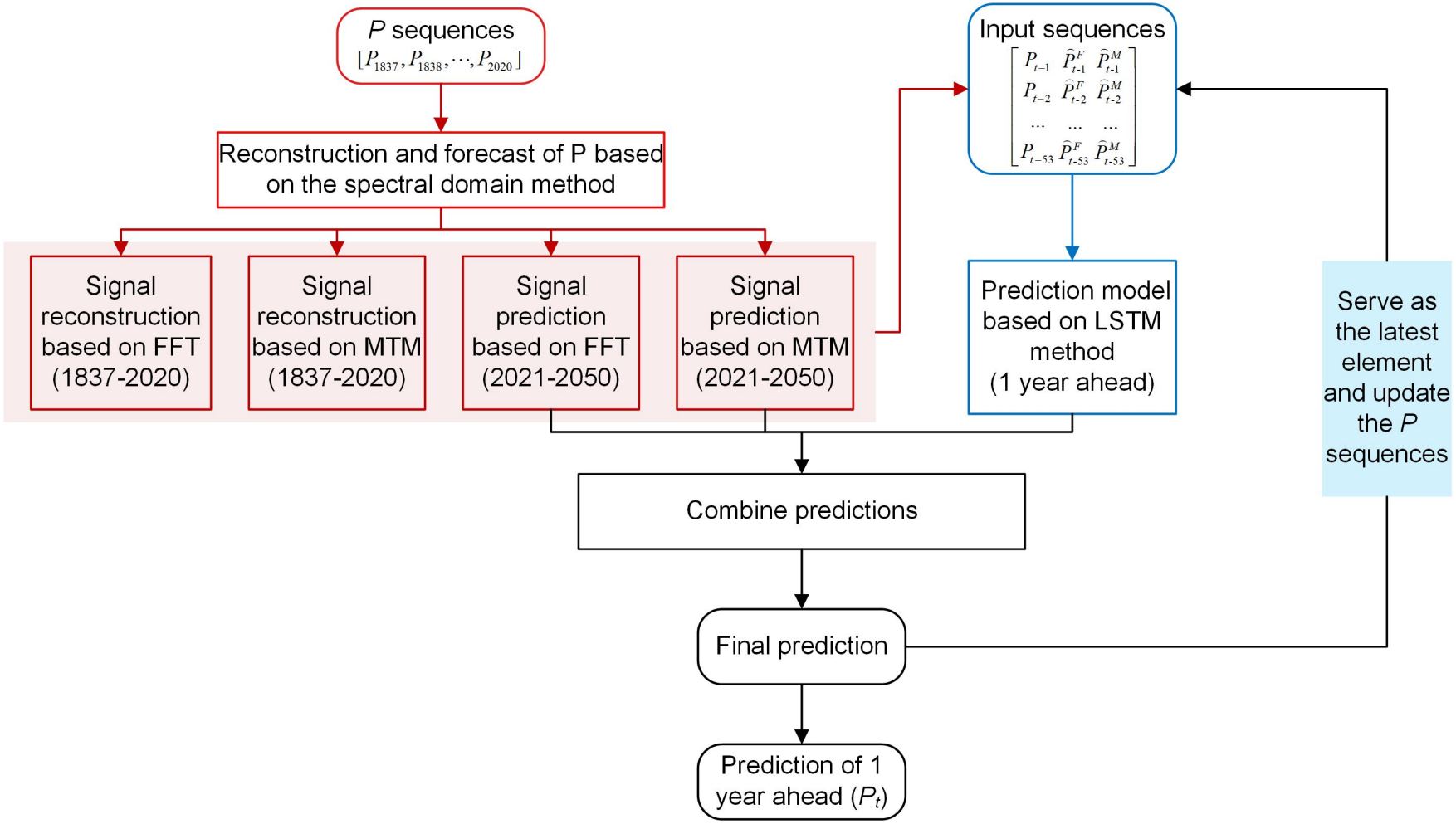

Extended Data Fig. 4.

The architecture of the proposed hybrid forecast model based on the LSTM and spectral domain approaches for predicting P. FFT and MTM denote the fast Fourier transform and multitaper methods, respectively.

Supplementary Materials for

Evaluation and prediction of the Effects of Planetary Orbital Variations to Earth's Temperature Changes

Mengmeng Cao[1]†, Kebiao Mao[1]*†, Sayed M. Bateni[2], Jing M. Chen[3,4], Essam Heggy[5,6], Jong-Seong Kug[7], Xinyi Shen[8]

Correspondence to: maokebiao@caas.cn

†These authors contributed equally to this work and should be considered co-first authors.

This PDF file includes:

Supplementary Text

1 The physical response of Earth's temperature to different orbits

1.1) The impact of the Earth's rotation on its temperature

Since the amplitude of the solar-induced temperature signal is negligible during the Earth's rotation [1], the quasi-sinusoidal diurnal variation (Fig. S1) in Earth's temperature (T) is mainly due to the uneven distribution of land and sea on the Earth's surface. For each point on Earth, the incoming solar radiation and outgoing longwave radiation changes during the day are mainly due to the Earth's rotation, causing the diurnal cycle of temperature. In this study, vernal equinoxes during the study period (1979−2020) were chosen for analyzing global hourly temperatures. We found large variations in the global temperature from 4 a.m. to 5 a.m., 7 a.m. to 8 a.m., 4 p.m. to 5 p.m. and 9 p.m. to 10 p.m. Fig. S2 shows the global distribution of the temperature difference between 4 a.m. and 5 a.m., 7 a.m. and 8 a.m., 4 p.m. and 5 p.m., and 9 p.m. and 10 p.m. The Earth's rotation highly affects the land surface temperature (LST), while the near-surface ocean temperature barely changes in the two consecutive hours. In Fig. S2, the warming (red color) of the land surface occurs from 5 a.m. to 2 p.m., while cooling (blue color) occurs from 2 p.m. to 5 a.m. of the next day. Fig. S3 indicates the globally averaged mean temperature difference between two consecutive UTC times on the vernal equinoxes during 1979−2020. The average global temperature varies significantly during 4 a.m. – 5 a.m., 7 a.m. – 8 a.m., 4 p.m. – 5 p.m., and 9 p.m. – 10 p.m. The globally averaged temperature change reaches its peak positive value between 7 a.m. and 8 a.m. (Fig. S3) because a large area (i.e., the entire African continent and the central and western parts of Eurasia) experiences warming (Fig. S2B). On the other hand, the globally averaged temperature change finds its peak negative value between 9 p.m. and 10 p.m. (Fig. S3) because most of the land on Earth undergoes cooling, except for northeastern Eurasia, southern Australia and northwestern North America (Fig. S2D).

1.2) The impact of the Moon on Earth's temperature

Fig. S4A shows the change in the global daily temperature from 1979 to 2020. The Earth's temperature in each year generally rises until it reaches its maximum around the middle of the year and then falls, which is mainly caused by the Earth's revolution around the Sun. This regular rising and falling pattern in the temperature is accompanied by slight irregular temperature fluctuations. We believe that these slight irregular fluctuations are mainly due to the changes in lunar forcing exerted on Earth.

Lunar tides and their cycles are well known and clearly observed in ocean records [2]. The lunar tidal cycles (which are generated by the gravitational effect of the Moon on Earth) may partially regulate ocean currents, thereby altering Earth's temperature [3]. The alternating asymmetric change in lunar gravitational forcing on the solid Earth and the ocean causes the periodic oscillation of crustal stress, which triggers local natural disasters and affects temperature changes locally and even globally [4-6]. Additionally, the periodic change in the lunar gravitational forcing on the Earth's atmosphere triggers the 27.3-day and 13.6-day atmospheric oscillatory systems and affects weather changes [7]. Moreover, the Earth's temperature is affected by reflection and infrared emission from the Moon [8,9].

By analyzing variations in daily lunar declination (δ), the distance between the Moon and the Earth, and the Earth's rotation from 1979 to 2020, we found further evidence of the effect of the Moon on the daily Earth's temperature. In this study, the daily length of day (LOD) values were used as

a measure of the angular velocity of the Earth, which was calculated as the difference between the astronomically determined duration of the day and 86400 SI seconds. In astronomy, δ is defined as the angle between the Moon's apparent path north or south of the celestial sphere and the celestial equator. Fig. S4B schematically depicts the Moon orbiting the Earth in an orbit tilted toward the celestial equator. Fig. S4C shows the temporal variations in δ, the temperature difference (D2) of two consecutive days and the LOD for 13 sidereal months from 1979−2020 (42 years). The variations in D2 and LOD show that they both have the same rising and falling trends, implying that the rotation of the Earth affects the variation in daily Earth's temperature. On the other hand, it was shown in Section 1.1 that Earth's rotation strongly affects the diurnal variation in Earth's temperature. Thus, if the rate of Earth's rotation changes regularly with the Moon's motion, it can further attest that the Moon can indirectly affect the daily global temperature fluctuations by affecting the Earth's rotation.

The Moon revolves every ~27.32 days in its elliptical orbit, which is known as the sidereal month. The change in LOD over the study period (i.e., 1979−2020) consists of two primary oscillations, namely, 27.3-day and 13.6-day oscillations, which correspond to the lunar sidereal period (Fig. S4C). The maximum (green arrows) LOD occurs when the Moon is on the celestial equator (δ = 0). In contrast, the minimum (orange arrows) occurs when the extreme lunar declinations appear in the northern or southern hemisphere ($\delta = \delta_L$) (Figs. S4B and 4C). Generally, changes in the lunar declination are approximately one day earlier than those of LOD. Additionally, we found that the rising and falling of LOD happen over 5 to 9 days and not necessarily a quarter of a sidereal month (Fig. S4C). All the short (13 days) and long (14-15 days) LOD cycles contain the Moon's perigee (P) and apogee (A), respectively. Theoretically, the Moon moves slower and faster near the apogee and perigee, respectively, which implies that LOD cycles with the apogee are slightly longer than those with the perigee. These findings show that lunar declination and the variable velocity of the Moon around the Earth affect the Earth's LOD. Meanwhile, all cycles with the perigee (P) have a higher peak than the adjacent cycles with the apogee (A), implying that the Moon's distance from the Earth affects the LOD. The LOD cycle with the highest peak arises when the perigee (P) is located near the peak and closer in time to new or full moons. All of the above findings clearly indicate that the lunar revolution around Earth is an important cause of daily variations in Earth's temperature.

1.3) The impact of the Earth's revolution on the Earth's temperature

Fig. S5 evaluates the effects of the Sun-Earth distance and the declination of the Sun on the Earth's temperature. It is found that the Earth's temperature is positively correlated with the Sun-Earth distance and the Sun's declination, with correlation coefficients (R^2) of 0.914 and 0.786, respectively. This happens because the distance-induced temperature signal is insignificant compared to that of solar declination, leading to a positive correlation between the Earth's temperature and its distance from the sun.

As noted in Section 1.1, Earth's temperature change is largely attributed to land's temperature change. The solar declination is positive from April to September, and the Sun's rays are directly over the northern hemisphere where larger land areas exist, causing the land to absorb more solar radiation and show a higher temperature. Once the solar declination reaches its maximum value, the solar radiation absorbed by the land approaches its peak, and the global temperature reaches a high value of 16.15 °C. From October to March, the solar declination is negative, and the Sun's rays shine directly on the southern hemisphere, where smaller land areas exist. Hence, the land

absorbs less solar radiation and exhibits a relatively lower temperature. That is why the Earth's temperature is highly correlated with solar declination (Fig. S5).

The Earth absorbs more solar radiation and has a higher temperature when it is closer to the Sun. However, due to the low eccentricity of the Earth's orbit, the Sun-Earth distance at the aphelion is only 1.033 times larger than that at the perihelion. The power of sunlight incident on the Earth's surface is inversely proportional to the square of the Sun-Earth distance [1,10]. Therefore, the sunlight power that reaches the Earth's surface at the perihelion is only 6.8% higher than that at the aphelion. The effect of the Sun-Earth distance on the Earth's temperature is insignificant compared to that of solar declination, leading to an inconsistency between the Earth's temperature and the Earth-Sun distance.

1.4) The impact of the motion of different planets on the Earth's temperature

Planetary motion directly and/or indirectly drives Earth's climate change on secular, millennium, and larger timescales [11-13]. Here, we performed a Fourier transform analysis of the annual mean temperature from 1836 to 2020 (185 years). The results showed that the global temperature has fluctuations in approximately 3.5, 9.1, 12.19, 18.28, 20.14, 29.92 and 61.2 years after 1836, which correspond to both the short-term oscillations of Earth's rotation and astronomical cycles (Table S1). This also implies that planetary motion may indirectly influence the interannual Earth's temperature by affecting the Earth's orbit and velocity.

2 Materials

In this study, hourly near-surface air temperature data (0.25°*0.25°) from 1979−2020 over the globe are obtained from the ERA5 dataset generated by the European Centre for Medium-Range Weather Forecasts (ECMWF). ERA5 is one of the most utilized datasets for climate studies [14]. The utilized global temperature data are generated by combining simulated and observed temperature data all over the world [15]. The daily, sidereal monthly, and annual mean temperatures are calculated using hourly data. The ERA5 dataset is available from 1979 and thus does not allow us to analyze changes in Earth's temperature on an interannual scale. To expand the temporal coverage of global temperature data, the daily mean temperature data from the NOAA-CIRES-DOE Twentieth Century Reanalysis version 3 (20CR V3) dataset were used for 1836–2015. Unlike the ERA5 dataset, which assimilates upper-air and satellite data, the 20CRV3 dataset assimilates only conventional near-surface observations (due to the lack of early satellite observations) to estimate temperature [16]. To keep the two datasets consistent, the ERA5 data were treated as a reference benchmark, and a linear regression matching technique was used to adjust the 20CR Version 3 data. The hourly, daily and sidereal monthly temperature data (1979−2020) derived from the ERA5 dataset were used to analyze and quantify the impact of different astronomical mechanisms on the Earth's temperature during a year. The annual mean temperature data (1836−2020) derived from both ERA5 and 20CRV3 were used to investigate the influence of the motion of all planets in the solar system on the Earth's temperature.

Daily atmospheric CO_2 concentration data from 1979 to 2020 were downloaded from the Scripps Institution of Oceanography archive (https://scrippsco2.ucsd.edu/data/atmospheric_co2/index.html). This dataset was generated by averaging in situ and flask CO_2 measurements from sampling stations. The sidereal monthly CO_2 concentrations (1979-2020) were derived from daily CO_2 data. The yearly atmospheric CO_2 records from 1836-2020 were also provided by the Scripps Institution of Oceanography. This dataset is mainly based on ice core data and the annual average of direct observations. The daily and yearly motions of the solar system objects were obtained from the

NASA Jet Propulsion Laboratory (JPL) ephemeris during 1979−2020 and 1836−2020, respectively (https://ssd.jpl.nasa.gov/horizons/app.html). The NASA JPL ephemeris provides the distance and velocity of the Earth relative to the Sun and the Moon, the distance and velocity of the center of mass of the Earth-Moon system relative to the Sun, and lunar declination. The 1979-2020 daily lunar phase information was obtained from the Fourmilab Switzerland website (http://www.fourmilab.ch/earthview/pacalc.html). The daily LOD data were obtained from the Earth's orientation parameters provided by the International Earth Rotation (IERS) Rapid Service/Prediction Centre at the U.S. Naval Observatory (https://www.iers.org/IERS/EN/DataProducts/EarthOrientationData/eop.html).

3 Robustness tests of methods

Fig. S6 A shows that Earth's temperature has increased since 1836 (red line). The upward trend in the Earth's temperature from 1836 to the present can be approximated by fitting a quadratic function to the Earth's temperature records. We can then approximately remove this upward trend using the quadratic fit function, which is shown by the histogram in Fig. S6 A. It can be seen that the histogram has two large and clear sinusoidal-like cycles during 1836−1964. Each of them has a period of approximately 61 years and a peak-to-trough amplitude of approximately 0.30-0.35 °C. In fact, there was a small change in greenhouse gas concentrations before the 1910s, and anthropogenic emissions also did not show any 61-year cycles before the 1940s [17]. Thus, the 61-year cycle temperature change should be caused by changes in the planet's orbit. Furthermore, the histogram was smoothed (black line) and shifted by 61 (red line) and $2 \times 61 = 122$ (blue line) years (see Fig. S6B). A shift of 61 years was chosen to be consistent with the highest temperature period in Table S1. Fig. S6B shows that the oscillations of Earth's detrended temperature among the 1850−1910, 1910−1970 and 1970−2020 periods (each period consists of 60 years) are fairly similar, and the Pearson coefficient of detrended temperatures among the three periods ranges from 0.74 to 0.86. It is evident that the 61-year cycle temperature change in Fig. S6B is caused by planetary orbital changes. Therefore, the Earth's detrended temperature in Fig. S6 A can represent the impact of the planet's orbit on the Earth's temperature change. In addition, the evident strong symmetry between the 1880–1920 and 1940–1980 periods indicates that the data in Fig. S6A before 1920 and 1940−1980 are more representative of the impact of the planet's orbit on the Earth's temperature change.

We converted the Earth's detrended temperatures in Fig. S6A to the effect of planetary orbits on the Earth's temperature changes in different years using 1836 as the benchmark. This can be done by subtracting the 1836 Earth's detrended temperatures from the Earth's detrended temperature records, which is shown with the blue line in Fig. S7. Then, we compared the result with that of our model (Fig. S7). The comparison shows that the results of both approaches are consistent during the study period, and they almost completely coincide before 1900. Moreover, a remarkable coincidence of the two curves is found from 1940−1980, which also corresponds to the more representative detrended temperatures in Fig. S6A. These outcomes show that the estimates of the effect of planetary orbits on the Earth's temperature changes from our model have high confidence.

4 Reconstructing and forecasting *P* using the spectral domain method

Since the effects of different planetary orbits on the Earth's temperature change exhibit obvious periodicity, there are significant fluctuations in P (Fig. 3B of Main Text). Thus, P can be reconstructed and forecasted reliably if its phases and frequencies are accurately determined. Based on harmonic approximation theory (i.e., harmonic approximation models can simulate

partial periodic time series [18,19]), we developed a harmonic approximation model for reconstructing and forecasting *P* using all statistically relevant oscillations that could be identified from its historical time series. The spectral domain approach can determine the periodic components embedded in a time series by computing the associated periods, amplitudes, and phases, and these individual periodic components can be combined to reconstruct and predict the future evolution of the time series. Thus, the relevant oscillations (i.e., periodic components) can be extracted using spectral analysis methods to build a harmonic approximation model. In this study, fast Fourier transform (FFT) and multitaper (MTM) methods were used to identify spurious spectral peaks and extract periodic components of *P* time series. It is worth mentioning that if the FFT spectral peaks were not verified by the MTM, they were excluded from the harmonic modeling of the *P* time series.

Based on the identified significant peaks of the *P* time series and information from the FFT and MTM decompositions, the associated periodic components were reconstructed in the time domain using the harmonic approximation model. The combination of oscillatory signals ($\hat{P}$) is written in continuous time as

$$\hat{P}_t = U + \sum_{m=1}^{M} A_m \sin(2\pi f_m(t - 1836) + \emptyset_m) \quad (1)$$

where *f*, *A*, and ϕ are the frequency, amplitude, and phase of the sine wave, respectively. *t* is the year, and *M* is the number of extracted significant peaks. U is set to 0.0567 and 0.0713 when the FFT and MTM frequencies are used, respectively.

Figs. S8 A and B show reconstructed *P* values from Equation 1 based on the information from the FFT and MTM decompositions, respectively. In addition, the periodic components obtained from the FFT and MTM spectral peak frequencies are shown in the same figure. It is evident that both approaches can reproduce the oscillations in *P* well, and thus, both methods can be used to predict *P*.

5 Forecasting *P* based on the LSTM method

LSTM is a recurrent neural network that is capable of learning long-term dependencies between samples in a sequence by updating states based on both the inputs for the current time step and network states of what was output in the prior time step. LSTM has the form of repeating modules of a neural network, and the repeating module is composed of four interactive parts, including a memory cell C, a forget gate f_t, an input gate i_t, and an output gate O_t (Fig. S9).

As illustrated in the second repeating module in Fig. S9, P_t is used as the input vector of LSTM in which the gates f_t, i_t, and O_t as well as the candidate cell state C'_t are all controlled by (P_t , h_{t-1}). f_t and i_t are then used to update the cell state C_t . O_t determines how much information is propagated to time step t+1. These gates are comprised of a sigmoid fully connected neural network layer and a pointwise multiplication operation. The working mechanism of the gates and information flow can be represented as follows:

$$f_t = \sigma(W_f \cdot [h_{t-1}, P_t] + b_f) \quad (2)$$

$$i_t = \sigma(W_i \cdot [h_{t-1}, P_t] + b_i) \quad (3)$$

$$C'_t = \tanh(W_c \cdot [h_{t-1}, P_t] + b_c) \quad (4)$$

$$C_t = f_t \odot C_{t-1} + i_t \odot C'_t \quad (5)$$

$$O_t = \sigma(W_o \cdot [h_{t-1}, P_t] + b_o) \quad (6)$$

$$h_t = O_t \odot \tanh(C_t) \tag{7}$$

where the transformations σ from inputs to i, f, and O all use sigmoid functions. W and b contain the corresponding network weights and bias parameters, respectively. h is the hidden state. The operation $\odot$ is elementwise multiplication (Hadamard product), and $\tanh(l)$ is the hyperbolic tangent function, which operates piecewise on each element of the vector l.

The hyperparameters of LSTM (e.g., the number of layers and the number of neurons in each layer) should be tuned to improve its performance. In this study, 10% of the data from the training dataset are selected randomly to tune the hyperparameters of LSTM via the Bayesian optimization method. We tested different numbers (from 1 to 5) of LSTM layers and combined the one, two, and three dense layers (also called the fully connected layers). Finally, we chose 4 layers (two LSTM layers and two dense layers) with 64, 32, 64 and 1 neurons. Meanwhile, we performed batch normalization after each hidden layer of the network. The best performance was obtained for a mini-batch size of 32. The mean square error (MSE) was used as the loss function. The Adam, RMSprop, AdaGrad, Nesterovs, SGD and Adadelta schemes were tested, and finally, the Adam scheme was adopted as the optimizer.

In addition to the hyperparameters of LSTM, the number of epochs and length of historical input data (timestep) affect *P* predictions. Fig. S10A shows that the magnitude of the loss function varies with the number of epochs in the LSTM model. It can be seen that the loss function remains almost constant for the epoch number of 300. Fig. S10B demonstrates the variations in the determination coefficient (R^2), the mean absolute error (MAE) and the root mean square error (RMSE) with timestep. The optimal timestep is set to 53, which means that we use the previous 53 years' input sequence to predict the 54th years' P.

Figures

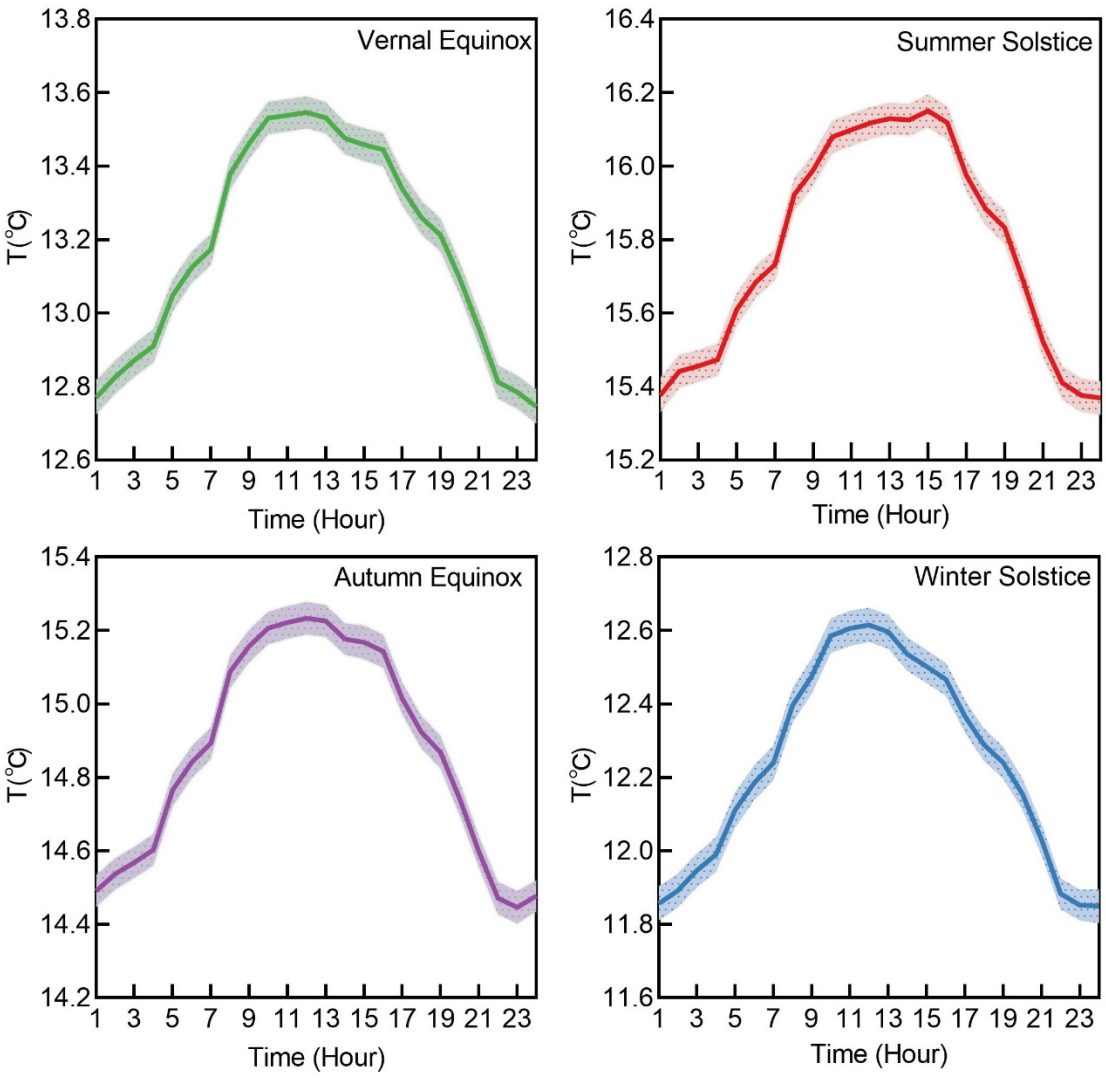

Fig. S1.

Diurnal cycle of Earth's temperature during the vernal equinox, summer solstice, autumn equinox and winter solstice during the study period. The band around each curve is the standard deviation of the temperature time series.

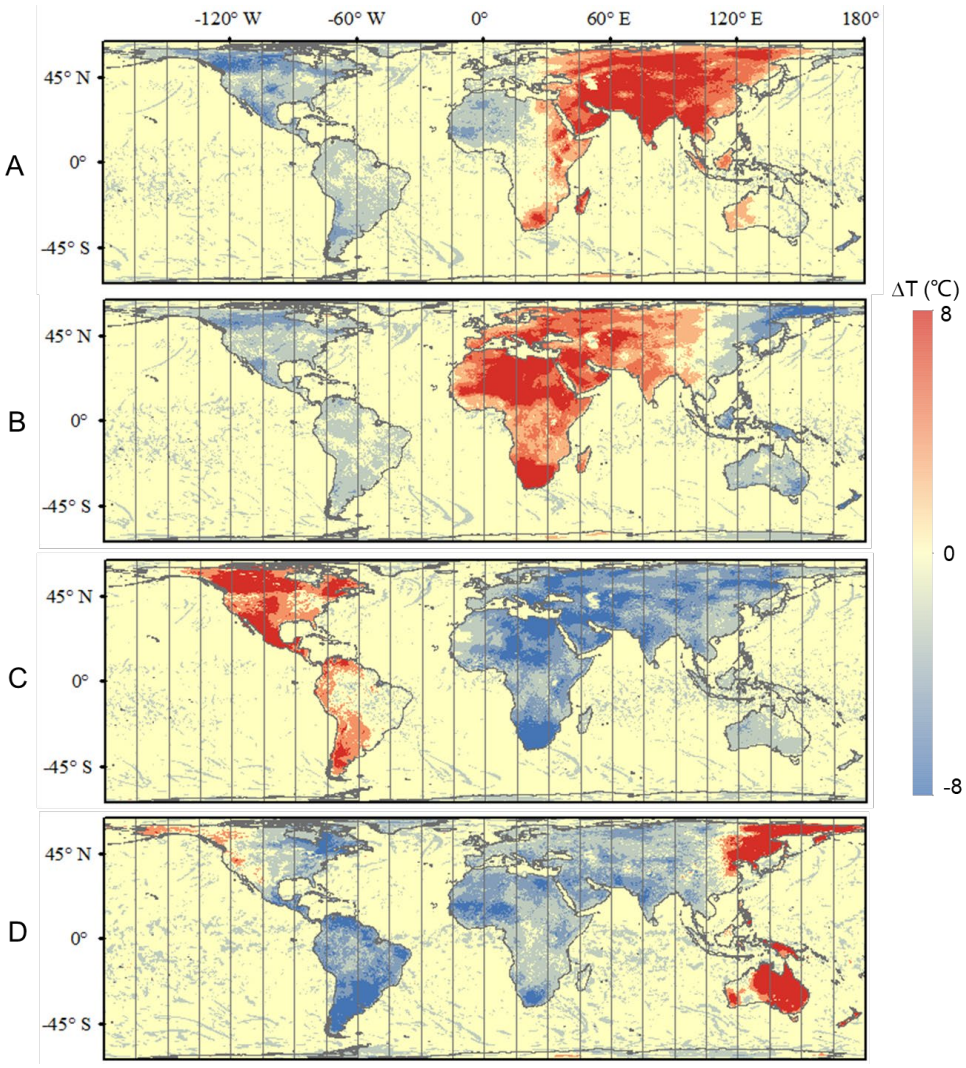

Fig. S2.

The mean temperature difference between two consecutive UTC times (**(A)** 5 and 4 UTC [T (at 5 UTC) – T (at 4 UTC)], **(B)** 8 and 7 UTC [T (at 8 UTC) – T (at 7 UTC)], **(C)** 17 and 16 UTC [T (at 17 UTC) – T (at 16 UTC)], and **(D)** 22 and 21 UTC [T (at 22 UTC) – T (at 21 UTC)]) on the vernal equinoxes from 1979-2020.

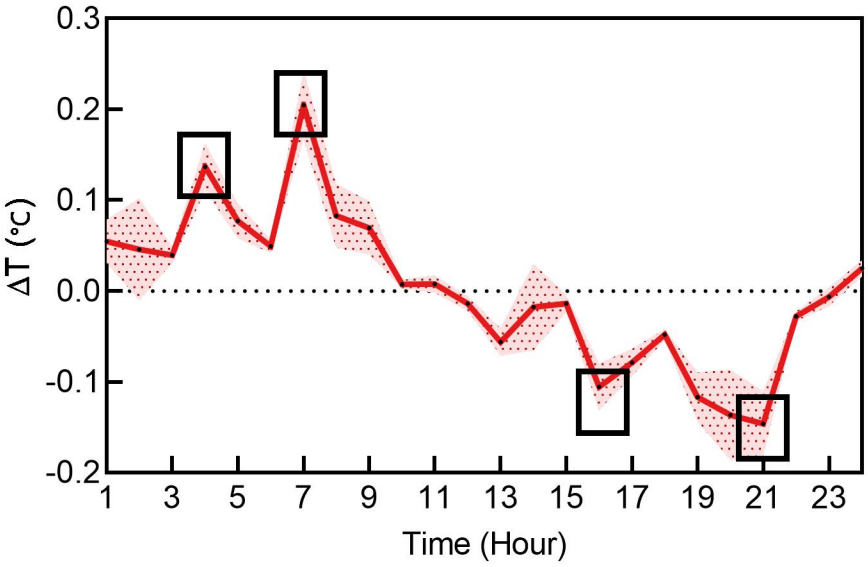

Fig. S3.

The spatially averaged mean temperature difference over the period 1979−2020 between two adjacent UTC times.

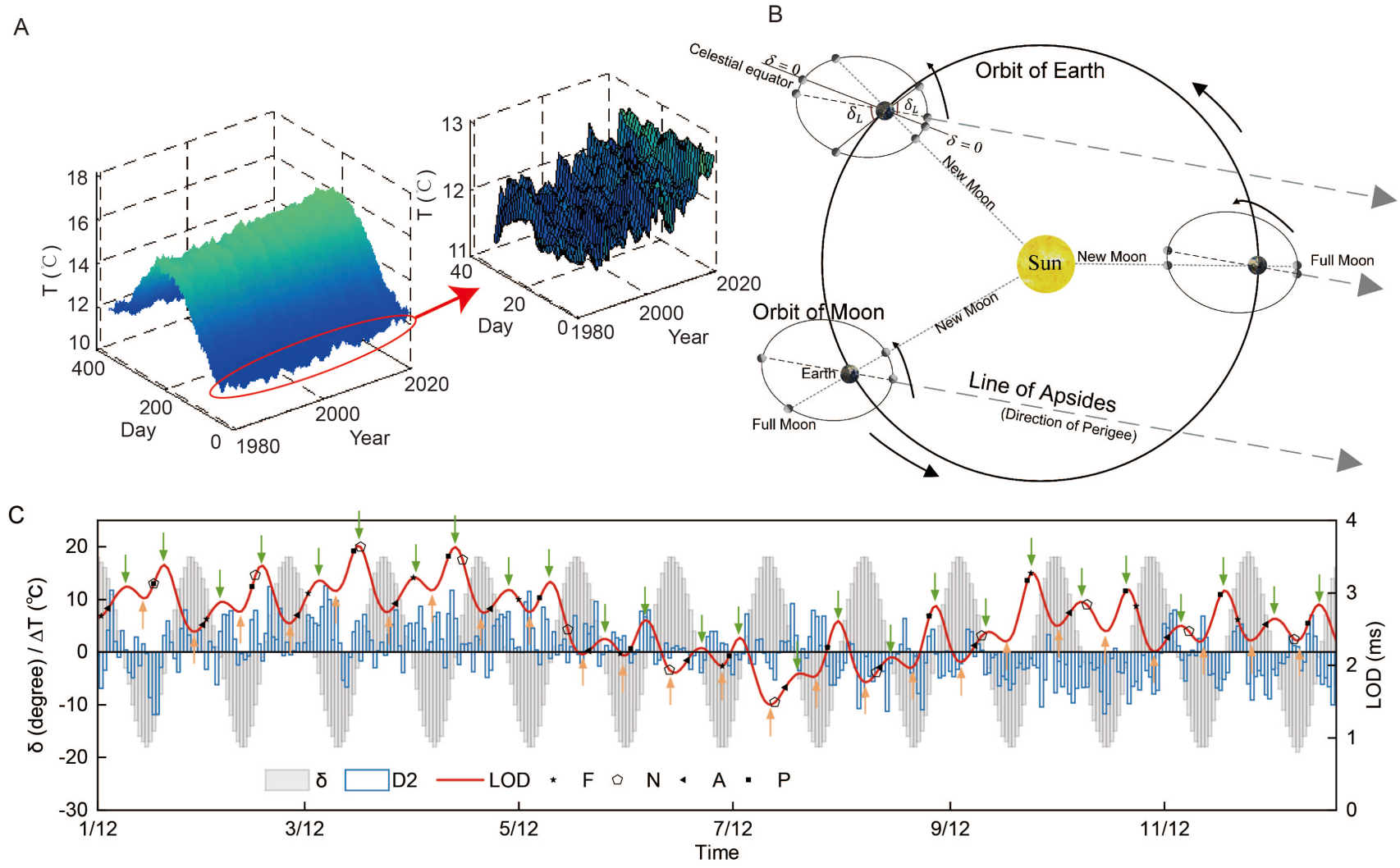

Fig. S4.

(**A**) Changes in the global daily temperature during 1979−2020. (**B**) A schematic diagram of the Moon orbiting the Earth in an orbit tilted to the celestial equator, which also depicts that the lunar declination, lunar phase and the distance of the Moon from the Earth all

change periodically during the Moon's orbit around the Earth. (**C**) The temporal variation of lunar declination, distance between the Moon and the Earth, LOD and temperature difference (D2) of two consecutive days from January 1979 to December 1979. The orange and green arrows represent the days on which the lunar declination (δ) is maximum and zero (i.e., the Moon is on the celestial equator), respectively. In astronomy, lunar declination is defined as the angle between the Moon's apparent path (north or south of the celestial sphere) and the celestial equator.

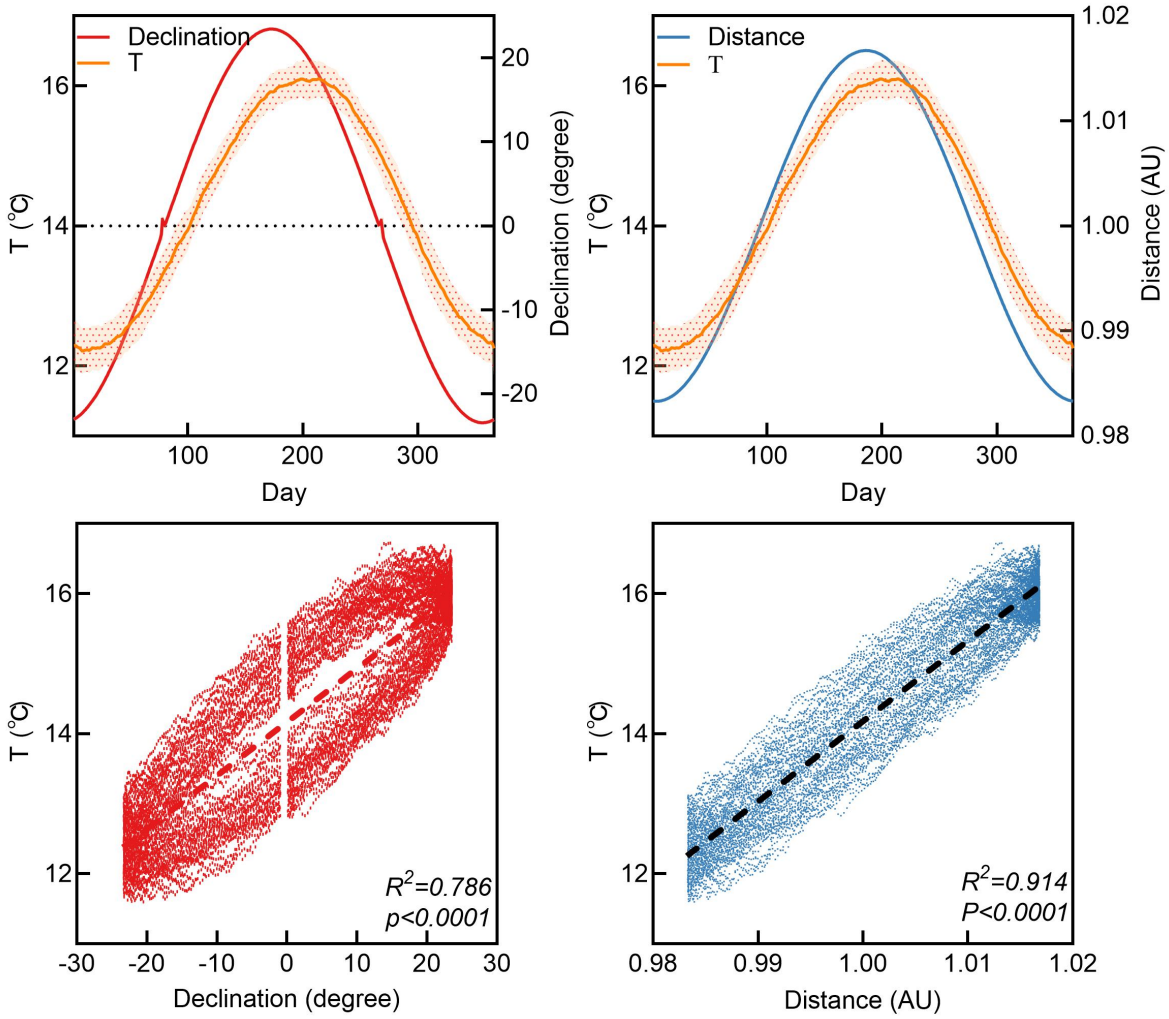

Fig. S5.

(Top row) Comparison of daily Earth's temperature data averaged over the period 1979−2020 with the solar declination (left column) and the Earth-Sun distance (right column). Orange bands represent the standard deviation of the daily Earth's temperature during the study period. (Bottom row) Scatterplot of the daily Earth's temperature data from 1979 to 2020 versus the solar declination and Sun-Earth distance.

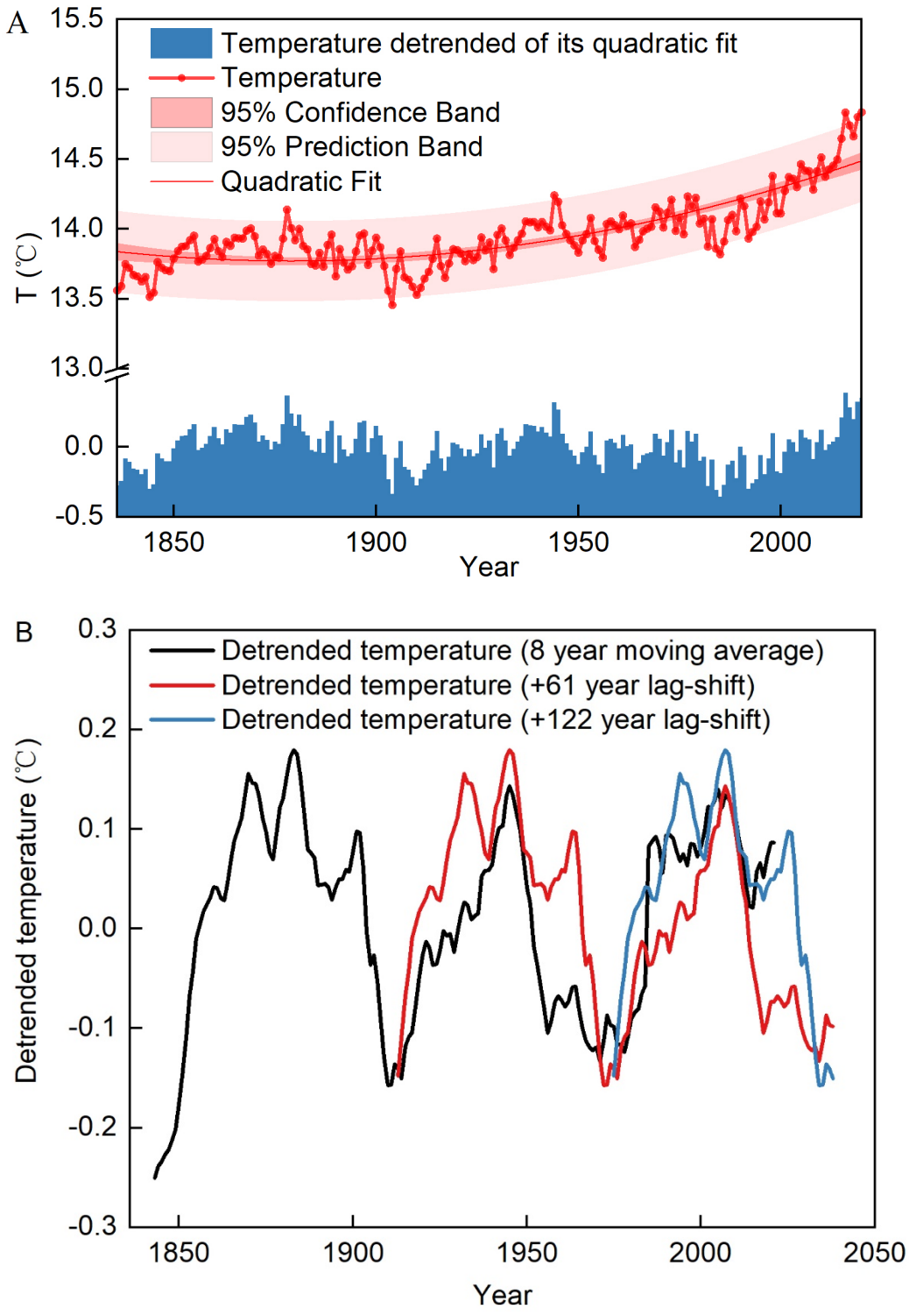

Fig. S6.

(**A**) Earth's temperature record and the detrended temperature of its quadratic fit; (**B**) eight-year moving average of the detrended temperature of its quadratic fit and plotted against itself shifted by 61 and 122 years.

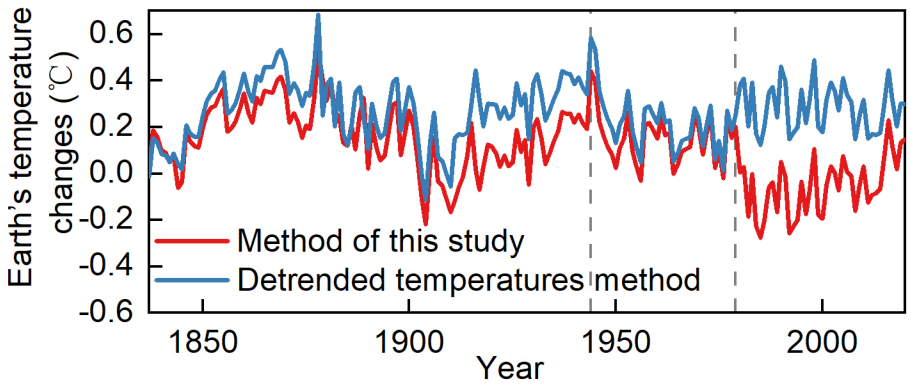

Fig. S7.

The effect of planetary orbits on global temperature changes in different years (using 1836 as the benchmark) based on the detrended temperatures method and the method of this study.

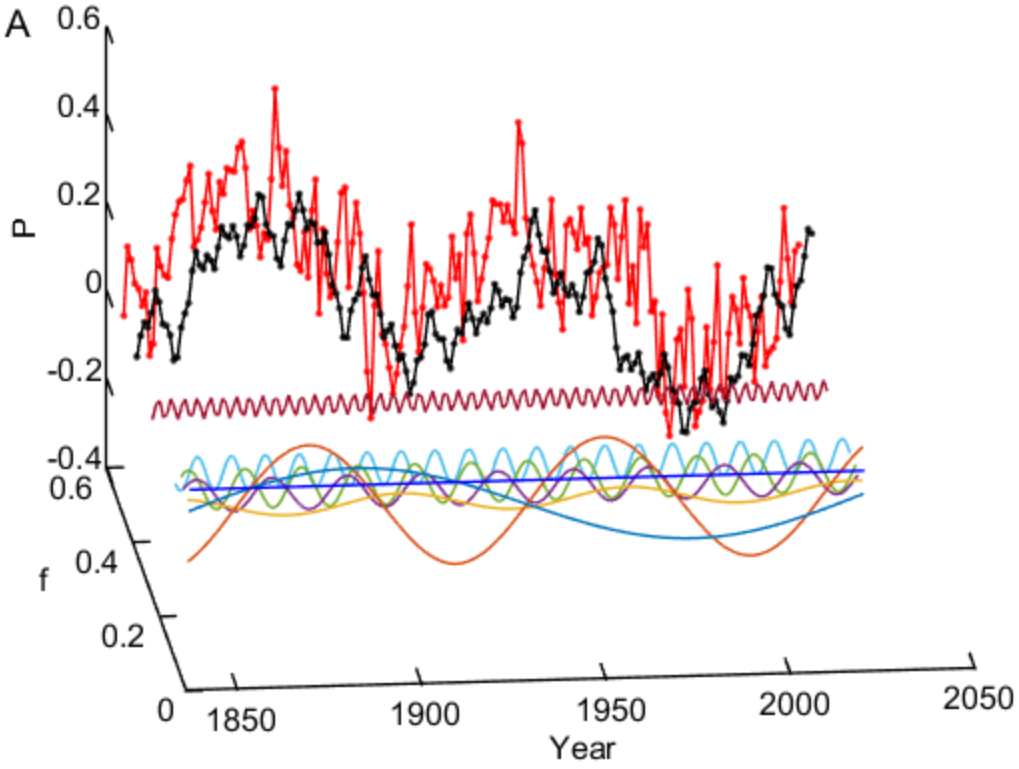
A
0.6
0.4
0.2
0
-0.2
-0.4
P
0.6
0.4
0.2
0
f
1850
1900
1950
2000
2050
Year

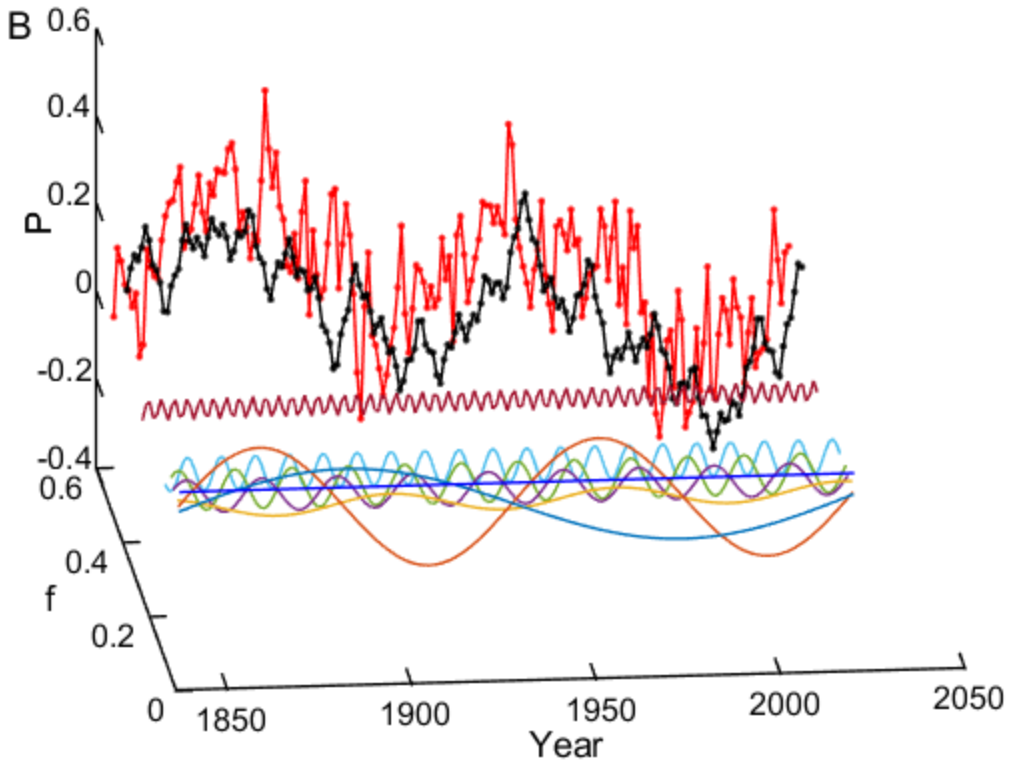
B
0.6
0.4
0.2
0
-0.2
-0.4
P
0.6
0.4
0.2
0
f
1850
1900
1950
2000
2050
Year

Fig. S8.

The effect of planetary orbits (P) on the Earth's temperature from 1837−2020 from the model of the methods section (red solid line with marker) and Equation (1) (black solid line with marker) using (A) the information from the FFT decomposition and (B) the information from the MTM decomposition. The remaining solid lines in A and B represent the periodic components obtained based on FFT and MTM spectral peak frequencies, respectively.

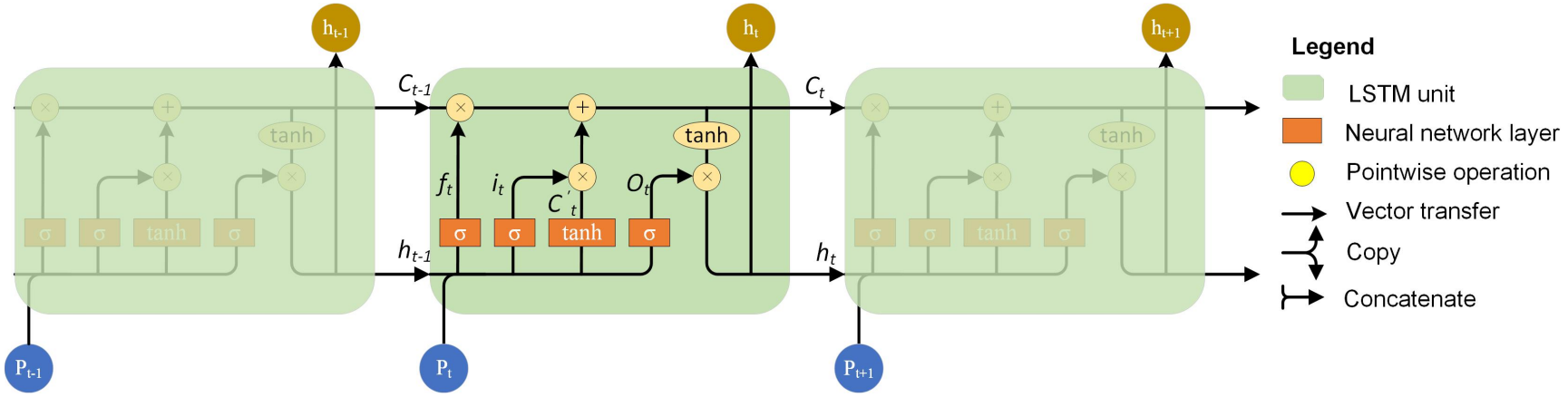

Fig. S9.
Structure of LSTM.

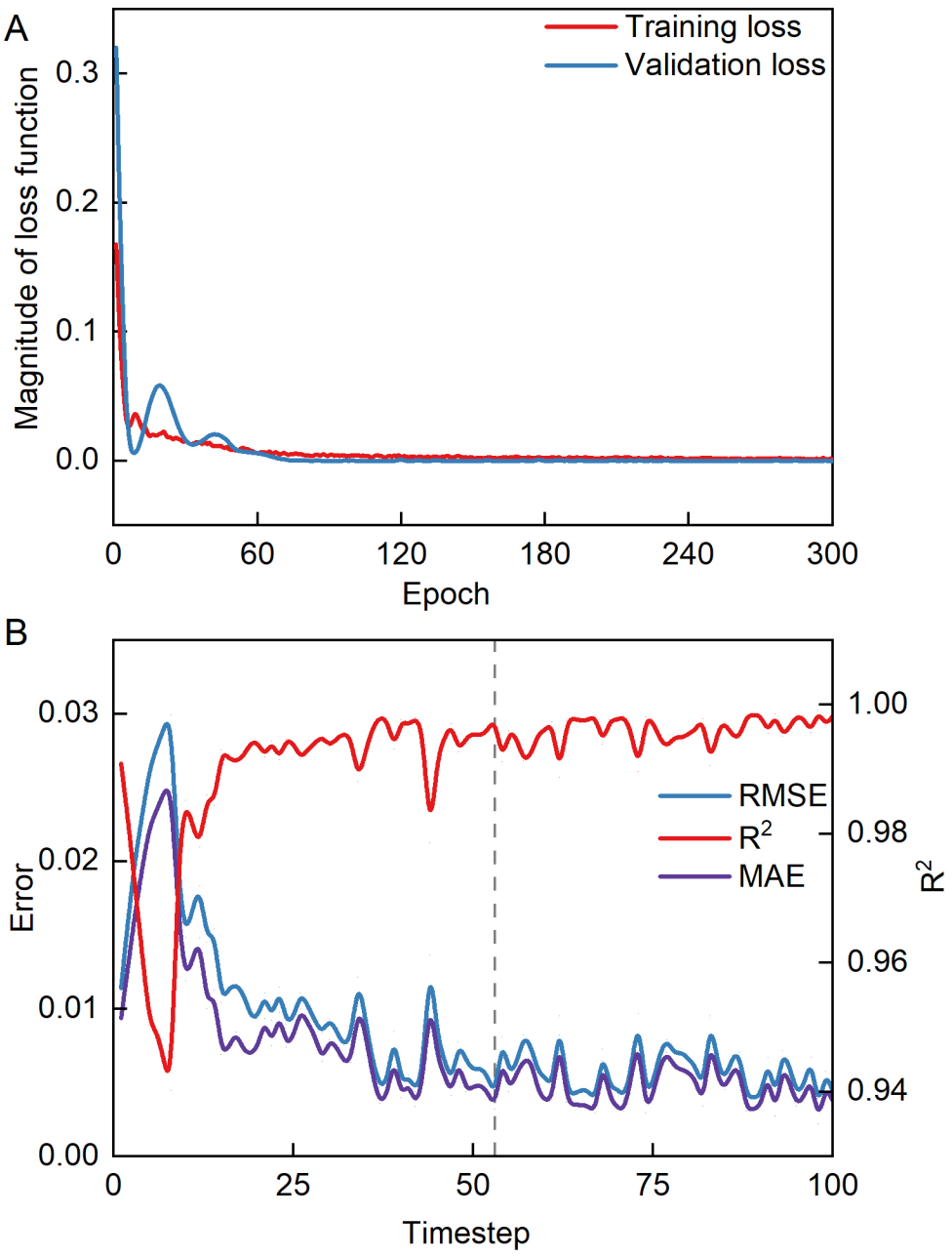

Fig. S10.

(**A**) The value of the loss function varies with the number of epochs in the LSTM for P prediction. (**B**) The relationship between the accuracy and the timestep of the LSTM.

Table S1.

The periods of the power spectrum of the Earth's temperature from 1836 to 2020 based on the FFT arithmetic corresponding to variation cycles of the Earth's rotation rate and astronomical periods.

Temperature periods (yr)	Earth rotation periods (yr)	Astronomical periods (yr)
3.5	4	Quasi-four yrs tidal cycle
9.1	9.2	The sunspot cycle (8.9-9.4 yrs); long-term lunar cycle (~9.1 yrs); the opposition-synodic cycle of Jupiter and Saturn (~10 yrs)
11.33-12.19	12.15	The sunspot cycle (9.9-13.035 yrs); the alignment cycle of Venus, Earth and Jupiter (~11 yrs); the period of Jupiter (11.86 yrs); the synodic period of Jupiter and Neptune (12.78 yrs)
18.28-20.14	18.6 19.855	The luni-solar node cycle (18.61 yrs); the synodic period of Jupiter and Saturn (19.858 yrs); the similar synodic period of Mercury (19.99 yrs)
29.92	29.783	The period of Saturn (29.42 yrs); the similar synodic period of Saturn (30.02 yrs); the period of polar shift (29.8 yrs)
~61	59.555	The sunspot cycle (~57.1 yrs); the repetition of the combined orbits of Jupiter and Saturn (~ 60 yrs)

Reference

1 Eddy, J. A., Gilliland, R. L. & Hoyt, D. V. Changes in the solar constant and climatic effects. *Nature* **300**, 689-693, doi:10.1038/300689a0 (1982).

2 McKinnell, S. M. & Crawford, W. R. The 18.6-year lunar nodal cycle and surface temperature variability in the northeast Pacific. *Journal of Geophysical Research: Oceans* **112**, doi:10.1029/2006JC003671 (2007).

3 Keeling Charles, D. & Whorf Timothy, P. Possible forcing of global temperature by the oceanic tides. *Proceedings of the National Academy of Sciences* **94**, 8321-8328, doi:10.1073/pnas.94.16.8321 (1997).

4 Mauk, F. J. & Johnston, M. On the triggering of volcanic eruptions by Earth tides. *Journal of Geophysical Research* **78**, 3356-3362 (1973).

5 Mauk, F. J. & Kienle, J. Microearthquakes at St. Augustine Volcano, Alaska, Triggered by Earth Tides. *Science* **182**, 386, doi:10.1126/science.182.4110.386 (1973).

6 Stroup, D. F., Bohnenstiehl, D. R., Tolstoy, M., Waldhauser, F. & Weekly, R. T. Pulse of the seafloor: Tidal triggering of microearthquakes at 9° 50′ N East Pacific Rise. *Geophysical Research Letters* **34**, doi:10.1029/2007GL030088 (2007).

7 Li, G. 27.3-day and 13.6-day atmospheric tide and lunar forcing on atmospheric circulation. *Advances in Atmospheric Sciences* **22**, 359-374, doi:10.1007/BF02918750 (2005).

8 Balling Robert, C. & Cerveny Randall, S. Influence of Lunar Phase on Daily Global Temperatures. *Science* **267**, 1481-1483, doi:10.1126/science.267.5203.1481 (1995).

9 Gee, H. Moonlight and global warming. *Nature*, doi:10.1038/news990624-9 (1999).

10 Willson, R. C. ACRIM3 and the Total Solar Irradiance database. *Astrophysics and Space Science* **352**, 341-352, doi:10.1007/s10509-014-1961-4 (2014).

11 Eddy John, A. The Maunder Minimum. *Science* **192**, 1189-1202, doi:10.1126/science.192.4245.1189 (1976).

12 Scafetta, N. Empirical evidence for a celestial origin of the climate oscillations and its implications. *Journal of Atmospheric and Solar-Terrestrial Physics* **72**, 951-970, doi:10.1016/j.jastp.2010.04.015 (2010).

13 Westerhold, T. *et al.* An astronomically dated record of Earth's climate and its predictability over the last 66 million years. *Science* **369**, 1383-1387, doi:10.1126/science.aba6853 (2020).

14 Graham, R. M., Hudson, S. R. & Maturilli, M. Improved Performance of ERA5 in Arctic Gateway Relative to Four Global Atmospheric Reanalyses. *Geophysical Research Letters* **46**, 6138-6147, doi:10.1029/2019GL082781 (2019).

15 Hersbach, H. *et al.* The ERA5 global reanalysis. *Quarterly Journal of the Royal Meteorological Society* **146**, 1999-2049, doi:10.1002/qj.3803 (2020).

16 Slivinski, L. C. *et al.* Towards a more reliable historical reanalysis: Improvements for version 3 of the Twentieth Century Reanalysis system. *Quarterly Journal of the Royal Meteorological Society* **145**, 2876-2908, doi:10.1002/qj.3598 (2019).

17 Hansen, J. *et al.* Climate simulations for 1880–2003 with GISS modelE. *Climate Dynamics* **29**, 661-696, doi:10.1007/s00382-007-0255-8 (2007).

18 Scafetta, N. Reconstruction of the Interannual to Millennial Scale Patterns of the Global Surface Temperature. *Atmosphere* **12**, doi:10.3390/atmos12020147 (2021).

19 Wang, T., Leung, H., Zhao, J. & Wang, W. Multiseries Featural LSTM for Partial Periodic Time-Series Prediction: A Case Study for Steel Industry. *IEEE Transactions on Instrumentation and Measurement* **69**, 5994-6003, doi:10.1109/TIM.2020.2967247 (2020).